Chemie der Erde 75 (2015) 89–104

Contents lists available at ScienceDirect

Chemie der Erde

journal homepage: www.elsevier.de/chemer

Gondwanan magmatism with adakite-like signature linked to Cu (Mo)-porphyry deposits from the San Rafael Massif, Mendoza Province, Argentina

Anabel L.R. Gómez [a,*], Nora A. Rubinstein [a], Víctor A. Valencia [b]

[a] Instituto de Geociencias básicas, aplicadas y ambientales de Buenos Aires (IgeBA) Departamento de Ciencias Geológicas, Facultad de Ciencias Exactas y Naturales, Universidad de Buenos-CONICET, Argentina
[b] School of Earth and Environmental Sciences Faculty, Washington State University, USA

ARTICLE INFO

Article history:
Received 21 October 2013
Accepted 17 November 2014
Editorial handling - U. Kelm

Keywords:
Gondwanan magmatism
Adakite-like signature
Cu-porphyry
San Rafael Massif
Argentina

ABSTRACT

The gondwanan magmatism in the San Rafael Massif, known as Choiyoi Magmatic Cycle, was emplaced during the inception of a magmatic arc setting during the early Permian. Two different sections can be differentiated in this volcanic sequence. The lower section (~281 up to ~265 Ma) consisting of andesites and dacitic to low-silica rhyolitic ignimbrites has geochemical characteristics that indicate a subduction zone setting. The upper section (~265 up to ~252 Ma) composed of rhyolitic ignimbrites and lava flows, dacitic to rhyolitic subvolcanics and alkalic basaltic andesites has geochemical characteristics transitional between subduction and continental intraplate settings. Several Cu–(Mo) porphyry deposits are genetically linked to the lower section (Infiernillo, San Pedro and La Chilca-Zanjón del Buitre). In this paper, we discussed the petrogenesis of the magmatism linked to the porphyry deposits from the San Rafael Massif. The petrogenetic analysis suggests that the lower section was produced in a thickened crust resulting in an adakite-like signature magmatism. The U/Pb LA-ICP-MS age of magmatic zircons from an intrusive associated to the San Pedro porphyry (263.1 ± 4.2 Ma) allowed confirming that the emplacement of Cu–Mo porphyry deposits in the San Rafael Massif occurred during the change in the geodynamical conditions from a transpressive to a transtensive tectonic regime.

1. Introduction

Adakite-like geochemical signatures within magmatic rocks have been related to the melting of mafic rocks equilibrated at high pressure (Defant and Drummond, 1990). This geochemical signature could be acquired following crustal thickening, slab melting of a young and hot plate, during flat slab subduction, fore-arc erosion or high-pressure fractional crystallization (Defant and Drummond, 1990; Atherton and Petford, 1993; Peacock et al., 1994; Rabbia and Hernández, 2000; Xu et al., 2002; Reich et al., 2003; among others).

Moreover, several authors have linked epithermal- and porphyry-type deposits such as those found in the Cenozoic of the Andes of Ecuador, Peru, Bolivia, Argentina and Chile to adakite-like rocks (Bray Du et al., 1995; Thiéblemont et al., 1997; Bissig et al., 2003; Reich et al., 2003; Chiaradia et al., 2004; Coldwell et al., 2005; Carrasquero et al., 2011).

The Gondwanan magmatism produced a large volume of volcanic and pyroclastic rocks along an NNW- to NW-trending belt extending between 28° and 42° S in Argentina and Chile (Nasi et al., 1985; Mpodozis and Kay, 1992; Llambías et al., 1993; Llambías and Sato, 1995; Kleiman and Japas, 2009; among others). In Argentina, these magmatic rocks named as the Choiyoi Magmatic Cycle (CMC) are exposed in the Frontal Cordillera (Llambías and Sato, 1995; Giambiagi and Martinez, 2008, among others), San Rafael Massif (Llambías et al., 1993; Kleiman and Japas, 2009 and references therein), North Patagonian Massif (Rapela and Llambías, 1985), Precordillera (Strazzere et al., 2006 and reference therein), Principal Cordillera (Dessanti, 1973), Chadileuvú Massif (Llambías et al., 2003), Sierras Australes (Grégori et al., 2003) and Sierras Pampeanas (Ramos et al., 1988).

Particularly, in the San Rafael Massif (SRM), two different sections can be distinguished within the volcanic sequence. The lower section (Early to Middle Permian) which was emplaced syntectonically with the San Rafael Orogeny (SRO) has geochemical features that indicate a magmatic arc setting (Llambías et al., 1993; Kleiman

* Corresponding author. Tel.: +54 114576 3300x313; fax: +54 114576 3300.
E-mail addresses: anabel@gl.fcen.uba.ar, anabelgomez7@yahoo.com.ar (A.L.R. Gómez), nora@gl.fcen.uba.ar (N.A. Rubinstein), victor.valencia@wsu.edu (V.A. Valencia).

http://dx.doi.org/10.1016/j.chemer.2014.11.001
0009-2819/

and Japas, 2009 and references therein). The upper section (Middle to Late Permian) which was emplaced during the Post-San Rafael extension (PSR) shows geochemical signatures that are transitional between subduction and continental intraplate settings (Llambías et al., 1993; Kleiman and Japas, 2009 and references therein).

Based on a Pb/Pb model age of 279 Ma and stratigraphic constraints, many hydrothermal ore deposits in the SRM were linked to the Gondwanan magmatism (Carpio et al., 2001; Rubinstein et al., 2004). The different styles of mineralization recorded in the upper and lower sections, respectively, were linked to the evolution of the Permian magmatic arc under a changing tectonic regime (Carpio et al., 2001). Several Cu–(Mo) porphyry deposits are hosted by the lower section (Fuschini, 1968; Delpino et al., 1993; Rubinstein et al., 2002, 2012; Gómez and Rubinstein, 2010a,b). Related to the upper section there are Mo porphyry prospects (Carpio et al., 2001) and epithermal low-sulfidation deposits (Rubinstein and Gargiulo, 2005; Gargiulo et al., 2007).

In this paper, we discuss the igneous petrogenesis and the geodynamic setting of the Gondwanan porphyry copper deposits from the SRM. The new geochemical and U/Pb LA-ICP-MS zircon crystallization geochronological results when integrated with available geological constraints, trace the transition from crustal thickening to a progressively extensional tectonic regime within a subduction-related setting and also reinforced the view of the link between adakite-like rocks and metalogenesis in subduction settings.

2. Regional geological setting

The SRM is located in the southern Mendoza Province, Argentina (Fig. 1a). Mesoproterozoic terrains are scarce in this area and include high-grade metamorphic rocks, granites, aplites and pegmatites of Grenvillian age (Cingolani and Varela, 1999). From the Ordovician to the Devonian, carbonatic and clastic sediments were deposited and later metamorphosed by the Famatinian Orogeny (Bordonaro et al., 1996). Carboniferous platform deposits were deposited over the metamorphosed Palaeozoic terrains and later folded during the SRO (Espejo and López Gamundi, 1994). During the Late Paleozoic (~284 Ma up to ~252 Ma, Rocha-Campos et al., 2011; Tickyj et al., 2014), a magmatic arc that was active on the western proto-margin of the Gondwana produced the CMC (Llambías et al., 1993). Following the CMC, syn-rift Triassic sequences were deposited associated with rhyolites, ignimbrites and basalts (Kleiman and Salvarredi, 2001).

The geological record from the Late Cretaceous to the Pliocene shows sequences of continental sedimentary rocks and volcanic-arc and back-arc products, including pyroclastic and siliceous to basaltic volcanic rocks, which were deformed during different phases of the Andean Orogeny. From the Miocene to Pleistocene, the geological record shows backarc deposits dominated by basalts interbedded with continental sedimentary rocks. The Miocene volcanics (Fig. 1a) have geochemical features that indicate a magmatic arc setting (Sepúlveda et al., 2007). On the other hand, the Holocene volcanic rocks (Fig. 1a) have an alkaline geochemical signature (Bermúdez et al., 1993; Sepúlveda et al., 2007) which was interpreted by Søager et al. (2013) in the Payenia volcanic province (southwest of the studied area) as a product of OIB mantle upwelling in a backarc setting.

2.1. Gondwanan magmatism in the San Rafael Massif

The lower section of the CMC corresponds to the Cochicó Group which consists mainly of andesites and dacitic to low silica rhyolitic ignimbrites with geochemical features indicative of an arc tectonic setting (Llambías et al., 1993). This section was emplaced during the SRO under a transpressional tectonic regime (Llambías et al., 1993; Kleiman and Japas, 2009 and references therein). The upper section includes the Quebrada del Pimiento, Cerro Carrizalito and Choique Mahuida and El Portillo Formations (Fig. 1a). These formations consist of rhyolitic ignimbrites and lava flows, dacitic to rhyolitic subvolcanics and alkaline basaltic andesites with geochemical characteristics transitional between subduction and continental intraplate settings. This section was emplaced during the PSR extension under a transtensional structural regime (Llambías et al., 1993; Kleiman and Japas, 2009). Although Agua de los Burros Formation is affected by the transpressional deformation of SRO, these volcanics are geochemically more similar to the upper section, therefore it is included in the upper section (Kleiman and Japas, 2009). Thus, the volcanic successions of the CMC reflect the transition from a convergence transpressional to a progressive extensional tectonic regime.

The extensional regime ends in Middle Triassic times (235.8 ± 2.0 Ma; Ottone et al., 2013) with the emplacement of the rift-related bimodal alkaline magmatism of the Puesto Viejo Formation (Llambías et al., 1993; Kleiman and Salvarredi, 2001).

Previous radiometric ages, obtained by K/Ar from whole rocks (Linares, 2007), suggest a middle Carboniferous (320 Ma) to early Jurassic (192 Ma) age for the CMC. Rocha-Campos et al. (2011) presented SHRIMP (sensitive high-resolution ion-microprobe) U/Pb ages of 281.4 ± 2.5 Ma (lower Permian) for the lower part of the Cochicó Group, 264.8 ± 2.3 Ma (middle Permian) for the Agua de los Burros Formation and 251.9 ± 2.7 Ma (Permian–Triassic boundary) for the Cerro Carrizalito Formation. More recently, U/Pb crystallization ages obtained by Tickyj et al. (2014) for a dacitic porphyry of the lower section and a granite intrusive of the upper section, both located ~100 km south-eastern of the San Pedro porphyry returned an age of 283.8 ± 0.98 Ma (Lower Permian) and 266.7 ± 1.0 Ma (Middle Permian), respectively. These new data constrain the age of the Gondwanan magmatism to the Permian with a spanning of ~30 Ma for the volcanic activity in the SRM.

2.2. Gondwanan porphyry Cu–(Mo) deposits from the San Rafael Massif

Three porphyry Cu–(Mo) deposits are hosted in the lower section of the CMC: Infiernillo, San Pedro and La Chilca-Zanjón del Buitre (Fig. 1a–d).

2.2.1. Infiernillo porphyry

This deposit (Fig. 1b) is hosted by the rhyolitic tuffs of the Cochicó Group composed of plagioclase, biotite and minor K-feldspar and amphibole in a recrystallized felsitic matrix where *fiammes* and shards are occasionally recognizable. The pyroclastic rocks are intruded by basaltic andesites dykes from the Quebrada del Pimiento Formation which are composed of plagioclase, olivine and amphibole phenocrysts in a pilotaxitic groundmass (Rubinstein et al., 2013).

The alteration zone only affects the pyroclastic rocks. It has an oval shape (Fig. 1b) with an NNE–SSW trend (Fuschini, 1968; Di Tommaso and Rubinstein, 2007). The core consists of an NNE oriented elliptical quartz plug sometimes with breccia texture that contains oxidized pyrite, scarce sericite and abundant hematite; locally it shows a boxwork texture. Surrounding the quartz plug, there is a potassic alteration zone which consists of pervasive K-feldspathization, silicification and minor biotitization (Fig. 2b). Outwards of the potassic alteration zone, there is a well-developed phyllic halo displaying intense bleaching (Fig. 2a). The halo shows a pervasive and veinlet-type silicification and pervasive sericitization. Abundant pyrite occurs as disseminated crystals and in veinlets. A late

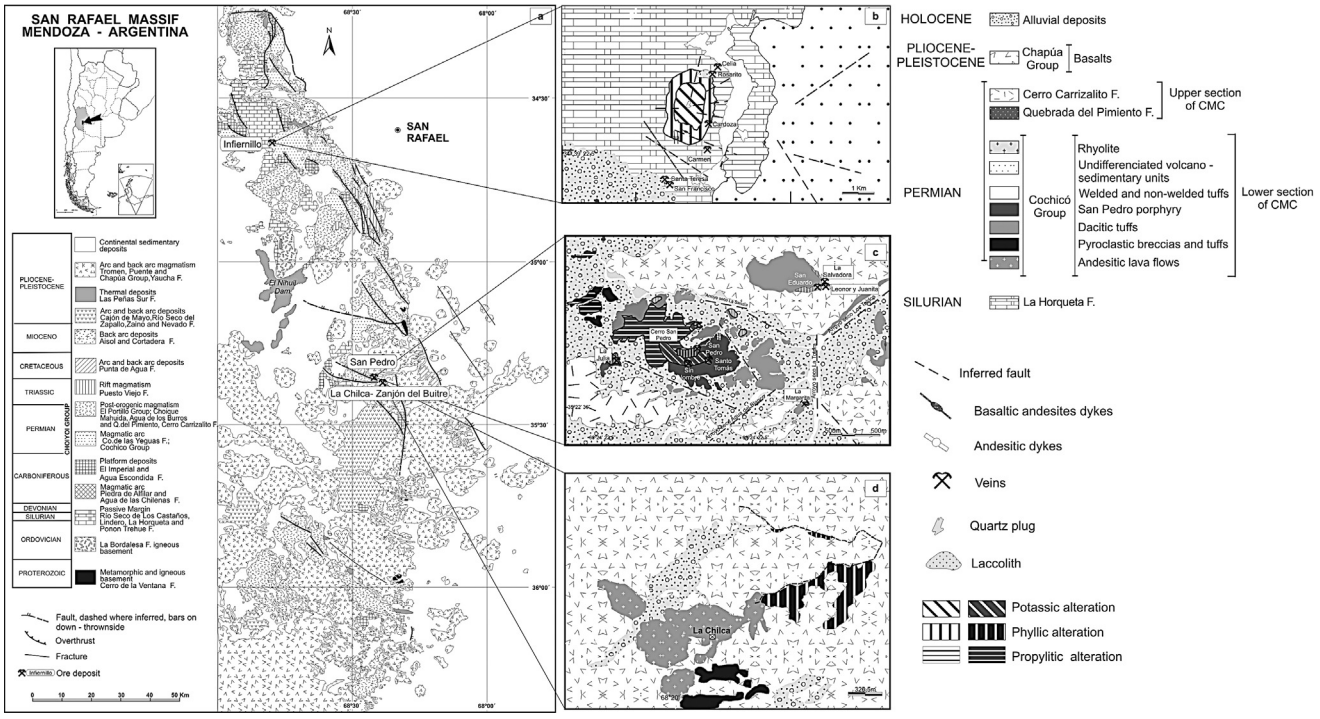

Fig. 1. (a) Geology of the San Rafael Massif showing the location of the porphyry Cu–(Mo) deposits. (b–d) Detailed maps of Infiernillo, San Pedro and La Chilca Zanjón del Buitre porphyries, respectively. Modified from Carpio et al. (2001), Gómez (2008, 2013) and Rubinstein et al. (2012).

carbonatization process overprints both the potassic and phyllic alteration (Di Tommaso and Rubinstein, 2007). The mineralization occurs as disseminated crystals and in quartz veinlets (Gómez and Rubinstein, 2010b). In the potassic alteration zone, the paragenetic sequence includes: bornite, chalcopyrite–molybdenite, pyrite, galena–sphalerite, chalcocite–covellite. In the phyllic zone, the paragenetic sequence includes: chalcopyrite, molybdenite and pyrite. Within or close to the outer border of the phyllic halo, small polymetallic veins with Pb–Zn–Ag mineralization crop out (Fig. 1b; Carpio et al., 2001). Surface geochemical analyses reveal almost superimposed anomalies of Cu and Mo located at the inner border of the phyllic halo (Fuschini, 1968; Di Tommaso and Rubinstein, 2007). Significant Ag and Au anomalies, up to 118 and 0.68 g/t, respectively, have also been detected (Zanettini and Carotti, 1993).

2.2.2. San Pedro porphyry

This deposit (Fig. 1c) is hosted by the Cochicó Group which consists of pyroclastic rocks intruded by a subvolcanic porphyry stock (San Pedro) and andesitic dykes (Figs. 1c and 2c). Outwards of the mineralized area, the Cochicó Group is intruded by basaltic andesites dykes from the Quebrada del Pimiento Formation (Fig. 1c). Volcanics of the Cerro Carrizalito Formation crop out to the south of the San Pedro porphyry (Fig. 1c).

The pyroclastic rocks of the Cochicó Group correspond mainly to a moderately welded massive dacitic tuff. They are composed of quartz, feldspars, micas and volcanic fragments in a felsitic matrix where recrystallized shards and *fiamme* are recognizable. The San Pedro Porphyry (SPP) consists mainly of a facies with porphyritic to granular texture and dioritic to tonalitic composition. It is composed of plagioclase, minor clinopyroxene, scarce biotite, magnetite and interstitial graphic intergrowth of quartz and K-feldspar. To the SE margin, scarce outcrops of a dacitic facies have been recognized. They display a porphyritic texture and are composed of plagioclase, biotite, quartz and amphibole phenocrysts in a very fine groundmass. Intruding the pyroclastic rocks and the SPP, there are andesitic dykes composed of plagioclase, amphibole and scarce K-feldspar phenocrysts in a fine plagioclase and quartz groundmass. The Quebrada del Pimiento dykes are composed of olivine and plagioclase phenocrysts in an intersertal groundmass.

The alteration zone covering the SPP and the surrounding pyroclastic rocks has an irregular shape (Fig. 1c). The potassic alteration is mainly developed in the central part of the SPP and shows an assemblage of K-feldspar, biotite, magnetite and quartz. It occurs pervasively and in veinlets (Fig. 2d).

Propylitic alteration occurs pervasively in the western part of the SPP and displays an assemblage of chlorite, epidote and carbonate. Chlorite–epidote veinlets are locally observed.

Weak phyllic alteration is irregularly distributed in the SPP and the surrounding pyroclastic rocks. It is marked by pervasive silicification and sericitization with disseminated pyrite and quartz–pyrite stockworks with minor chalcopyrite, sphalerite and galena. The phyllic alteration does not affect the andesitic dykes (see Fig. 1c). A late carbonatization process, locally pervasive but also present in veins, overprints both the potassic and phyllic alteration. Within or close to the potassic alteration zone, Cu–Pb–Zn–Ag-(Mo) veins (Fig. 1c) crop out (Rubinstein et al., 2002). Geochemical analyses yielded an average ore grade of 2.5% Cu and 542 ppm Mo (Davicino, 2008).

Based on the intrusion sequence and the mineralogy and the alteration patterns of the intrusions, the dioritic–tonalitic facies of the SPP is considered as an early-mineralization facies, whereas the andesitic dykes are considered post-mineralization. Although the link between the dacitic facies of the SPP and the mineralization is not clear, because of its mineralogy and location, it could be considered as genetically linked to the mineralization.

2.2.3. La Chilca-Zanjón del Buitre porphyry

La Chilca-Zanjón del Buitre is located at 7.5 km to the southeast of the SPP (Fig. 1a). The alteration zone consists of two

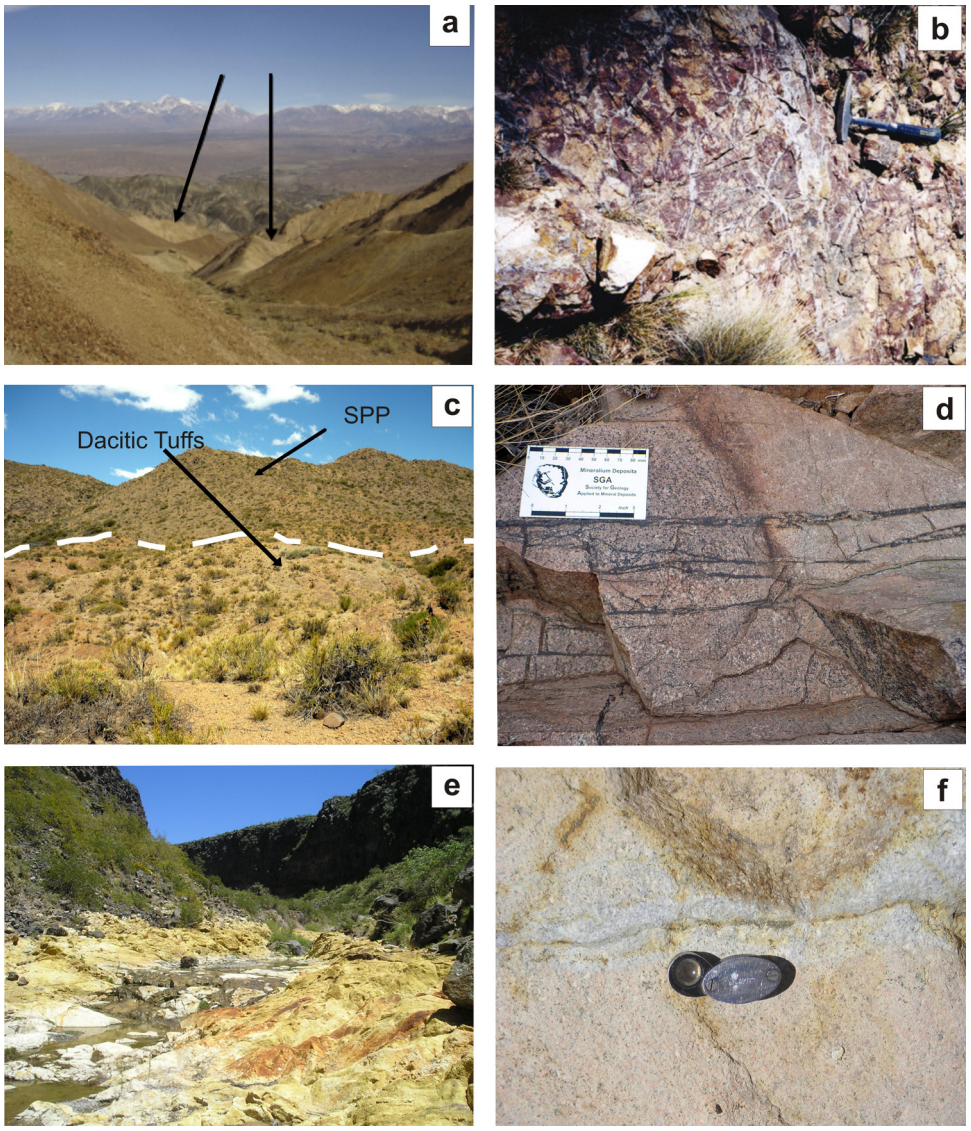

Fig. 2. Alteration zones view. (a) Infiernillo. Regional view of phyllic alteration showing intense bleaching. (b) Infiernillo. Potassic alteration and silicification in stockwork structure. (c) San Pedro. Regional view of the SPP and dacitic tuffs (Cochicó Group). (d) San Pedro. Pervasive K-feldspar alteration zone with quartz–magnetite veinlets. (e) La Chilca-Zanjón del Buitre. Phyllic alteration area. (f) La Chilca-Zanjón del Buitre. Pyrite veinlets.

belts about 1 km in length with an ENE strike which are hosted by ignimbrites of trachyandesitic composition interbedded with tuffaceous sandstones and andesitic lava flows (Fig. 1d). The ignimbrites are composed of feldspars, quartz, biotite and amphibole clasts along with scarce volcanic fragments in a felsitic matrix with recrystallized *fiammes*. The lava flows have a porphyritic texture and consist of plagioclase and amphibole in a groundmass with pilotaxitic texture. This volcaniclastic sequence is intruded by dacitic and andesitic subvolcanic bodies composed by feldpars (plagioclase and K-feldspar) with subordinate biotite, quartz and amphibole phenocrysts in a felsitic groundmass (Rubinstein et al., 2012).

The altered area consists of a potassic zone with pervasive alteration and a paragenesis of K-feldspar–quartz–magnetite partially overprinted by a pervasive phyllic alteration with an assemblage of quartz–muscovite–pyrite–(rutile) and pyrite–(quartz) veins (Figs. 1d, 2e and f). A late carbonatization process overprints both the potassic and phyllic alteration. Outside the alteration zone, pyrite–chalcopyrite–galena–sphalerite veins with a quartz gangue are observed. Chemical analyses indicate moderate Ag and Au anomalies and small anomalies of Cu, Mo, Pb and Zn (Rubinstein et al., 2012).

3. Methods and analytical procedures

Twenty-one rock samples from the SPP were analyzed for major and trace elements at Actlabs (Canada) and SGS (Peru) laboratories.

One mineralized sample from the early-mineralization SPP facies was selected for zircon U/Pb dating. Heavy mineral concentrates of the <350 μm fraction were separated using traditional techniques at ZirChron LLC. Zircons from the non-magnetic fraction were handpicked under the microscope and mounted in a 1-inch diameter epoxy puck and slightly ground and polished to expose the surface and keep as much material as possible for laser ablation analyses. LA-ICP-MS U/Pb analyses were conducted at Washington State University prior to cathodoluminescence imaging using a New Wave Nd:YAG UV 213-nm laser coupled to a ThermoFinnigan Element 2 single collector, double-focusing, magnetic sector ICP-MS. Operating procedures and parameters are a slight modification of Chang et al. (2006). Laser spot size and repetition rate were

Table 1
U/Pb isotopic data for zircons crystal from SSP obtained by LA-ICPMS.

CSP0913	U (ppm)	Th/U	$^{238}U/^{206}Pb$	1 sigma (% error)	$^{207}Pb/^{206}Pb$	1 sigma (% error)	$^{206/238}$ age	1 sigma (abs err)	$^{207}U/^{206}Pb$ age	1 sigma (abs err)	Best age	1 sigma (abs err Ma)
nora_32	300	0.28	23.5875	1.97	0.0517	1.47	267.7	5.2	270.5	33.4	267.7	5.2
nora_31	344	0.43	23.0370	1.95	0.0522	1.38	273.9	5.2	292.3	31.3	273.9	5.2
nora_30	325	0.27	22.4295	2.10	0.0586	1.40	281.2	5.8	553.8	30.2	281.2	5.8
nora_29	279	0.32	24.1438	1.91	0.0521	1.46	261.6	4.9	290.9	33.1	261.6	4.9
nora_28	90	0.75	16.9673	2.32	0.0570	1.90	369.2	8.3	491.9	41.4	369.2	8.3
nora_27	374	0.43	9.3635	4.28	0.0832	1.16	654.1	26.6	1274.9	22.5	654.1	26.6
nora_26	839	0.33	6.5451	2.06	0.0847	1.14	916.6	17.6	1309.3	22.1	1309.3	22.1
nora_24	298	0.21	25.6360	1.66	0.0522	1.28	246.7	4.0	310.9	30.2	246.7	4.0
nora_23	212	0.20	25.0660	1.68	0.0525	1.53	252.2	4.1	308.0	34.6	252.2	4.1
nora_22	116	0.29	23.7907	1.69	0.0521	1.90	265.4	4.4	290.1	42.9	265.4	4.4
nora_21	194	0.22	23.8677	1.69	0.0514	1.49	264.6	4.4	257.8	33.8	264.6	4.4
nora_20	275	0.26	25.3897	1.58	0.0512	1.40	249.0	3.9	281.7	32.1	249.0	3.9
nora_19	210	0.22	25.2793	1.81	0.0492	1.66	250.1	4.4	203.3	37.9	250.1	4.4
nora_18	115	0.13	5.8719	1.68	0.0751	1.12	1013.8	15.7	1089.3	22.7	1089.3	22.7
nora_17	324	0.38	24.7924	1.82	0.0515	1.31	254.9	4.5	275.4	29.3	254.9	4.5
nora_16	302	0.37	23.8265	1.57	0.0523	1.25	265.0	4.1	305.9	28.4	265.0	4.1
nora_15	287	0.28	24.0579	1.76	0.0530	1.32	262.5	4.5	330.3	29.8	262.5	4.5
nora_14	333	0.26	23.9694	1.59	0.0507	1.32	263.5	4.1	235.1	30.6	263.5	4.1
nora_13	299	0.30	24.4727	1.67	0.0526	1.30	258.2	4.2	322.1	29.8	258.2	4.2
nora_11	260	0.22	23.8730	1.55	0.0527	1.28	264.5	4.0	315.3	28.7	264.5	4.0
nora_10	211	0.93	24.2409	2.25	0.0515	1.81	260.6	5.7	263.7	40.9	260.6	5.7
nora_9	664	0.38	18.6541	2.06	0.0525	1.38	336.6	6.8	311.9	31.2	336.6	6.8
nora_8	298	0.24	24.3653	2.14	0.0519	1.61	259.3	5.4	298.6	36.6	259.3	5.4
nora_7	347	0.20	23.5893	2.16	0.0522	1.74	267.6	5.7	396.5	38.9	267.6	5.7
nora_6	502	0.38	23.9667	2.66	0.0593	1.82	263.5	6.9	576.7	39.1	263.5	6.9
nora_5	339	0.29	23.7154	2.09	0.0533	1.58	266.2	5.4	341.8	35.4	266.2	5.4
nora_4	423	0.56	24.0987	1.99	0.0522	1.52	262.1	5.1	292.7	34.3	262.1	5.1
nora_3	318	0.31	23.4787	2.07	0.0524	1.50	268.9	5.5	307.4	33.9	268.9	5.5
nora_2	270	0.19	23.6829	2.06	0.0524	1.63	266.6	5.4	308.3	37.1	266.6	5.4
nora_1	315	0.61	23.8069	2.07	0.0552	1.58	265.2	5.4	424.9	35.0	265.2	5.4

30 μm and 10 Hz, respectively. He and Ar carrier gases delivered the sample aerosol to the plasma. Each analysis consists of a short blank analysis followed by 250 sweeps through masses 204, 206, 207, 208, 232, and 238, taking approximately 30 s. Time-independent fractionation was corrected by normalizing U/Pb and Pb/Pb ratios of the unknowns to the zircon standards (Chang et al., 2006). U and Th concentration were monitored by measuring the concentration of 610 NIST glass. Two zircon standards were used: Plesovice, with an age of 338 Ma (Sláma et al., 2008) and FC-1, with an age of 1099 Ma (Paces and Miller, 1993). U-Pb ages were calculated using Isoplot (Ludwig, 2003). U–Pb zircon crystallization age errors are reported using quadratic sum of the weighted mean error plus the total systematic error for the set of analyses (Valencia et al., 2005).

4. Geochronology

Zircon crystals of the analyzed sample (CSP0913) have mainly euhedral external analyzed morphologies and zoned inner structures typical of igneous zircons. Disruptions of the inner structure,

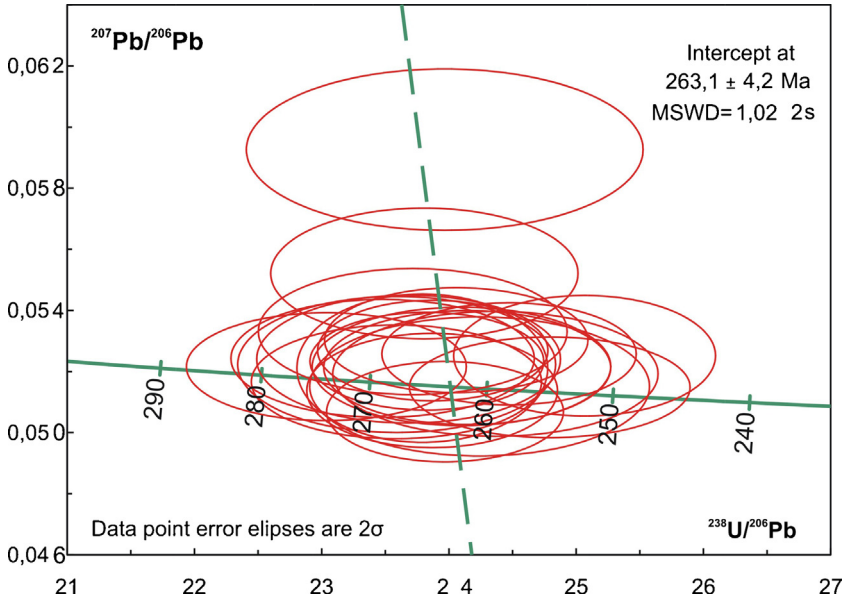

Fig. 3. Tera Wasserburg diagram of LA-ICP-MS analyses of zircons from the SPP.

Table 2
Major (wt%) and trace element (ppm) contents of the CMC from the mineralized areas (San Pedro, Infiernillo and La Chilca-Zanjón del Buitre porphyries and Don Sixto epithermal ore deposit) and unmineralized areas of the SRM.

Mineralized areas	San Pedro Porphyry																		
CMC	Lower Section																		
Stratigraphic Unit	Cochicó Group																		
Lithology	SPP											Andesitic dykes		Dacitic Tuffs					Andesitic breccia
Samples	CSP0940†	CSP0943†	CSP093†	CSP0913†	CSP094†	CSP0950*	CSP0951*	CSP01089†	CSP0108†	CSP015*	CSP0944*	CSP0945†	CSP0941†	CSP096†	CSP095†	CSP0935†	CSP098†	CSP0912†	
Latitude S	35° 21′51.05″	35° 21″ 51.0″	35° 20″ 50.08″	35° 21″ 39.03″	35° 20″ 50.08	35°21′58.41″	35°21′57.25″	35°21′59.85″	35° 22.352″	35° 21.633″	35°21′50.04″	35° 21″ 47.04″	35° 21″ 51.05″	35° 21″ 23.8″	35° 21″ 23.8″	35° 22″ 36.01″	35° 21.583	35° 21″ 23.5″	
Longitude W	68° 24′58″	68 ° 24″56.02″	68° 26″ 23.09″	68° 26″ 0.01″	68° 26′23.09″	68°21′16.78″	68°25′17.89″	68°25′12.00″	68 24.174″	68° 25.100″	68°24′51.09″	68° 24″ 48.06″	68° 24″ 58″	68° 25″ 45.9″	68° 25″ 45.9″	68° 23″ 51.02″	68° 26.138″	68 26″ 16.2	
SiO_2	63.48	67.37	63.01	58.99	62.80	61.95	61.18	64.20	64.14	64.93	63.53	62.09	63.95	59.32	61.11	63.00	62.02	56.33	
TiO_2	0.48	0.59	0.56	0.72	0.55	0.57	0.56	0.60	0.50	0.56	0.55	0.69	0.57	0.57	0.54	0.60	0.59	0.75	
Al_2O_3	14.80	16.51	16.90	18.07	16.57	14.51	14.84	15.54	15.17	14.64	14.61	15.28	16.30	15.68	15.71	16.17	16.01	16.02	
FeO	–	–	–	1.20	–	–	–	–	–	–	–	–	–	–	–	–	–	–	
Fe_2O_3	2.31	1.98	4.32	5.70	4.57	5.04	4.74	4.73	3.78	3.97	1.83	3.93	2.86	4.44	4.28	4.04	4.99	6.62	
MnO	0.12	0.03	0.07	0.09	0.09	0.15	0.14	0.08	0.05	0.03	0.07	0.11	0.08	0.07	0.11	0.13	0.03	0.07	
MgO	0.80	1.17	1.36	1.52	1.23	1.94	1.55	1.54	0.52	1.41	1.38	0.95	0.12	0.44	0.53	0.89	1.41	2.58	
CaO	4.76	1.84	3.66	4.73	2.76	3.16	5.00	3.32	3.57	0.98	2.94	3.85	3.25	5.75	4.31	3.25	2.86	4.78	
Na_2O	6.27	4.71	4.98	4.89	5.24	4.87	5.75	4.76	4.04	4.90	7.37	5.44	5.21	4.42	4.44	4.59	5.64	5.84	
K_2O	0.95	2.94	2.98	2.64	3.21	3.09	2.24	3.27	3.30	3.89	1.56	2.98	3.27	2.30	2.23	3.20	2.58	0.98	
P_2O_5	0.22	0.25	0.22	0.27	0.26	0.24	0.22	0.22	0.20	0.26	0.23	0.30	0.26	0.23	0.21	0.32	0.26	0.30	
LOI	5.90	2.38	2.73	1.66	2.11	1.63	0.81	2.68	4.39	2.27	3.63	4.21	4.05	6.55	5.83	4.46	3.61	5.51	
Ba	41.00	1544.00	1359.00	1421.00	1539.00	1047.20	668.60	1351.00	1198.00	1977.50	669.10	1286.00	1464.00	1254.00	1611.00	1496.00	976.00	289.00	
Rb	20.00	49.00	62.00	54.00	67.00	73.60	38.60	76.00	77.00	70.10	31.70	52.00	49.00	52.00	52.00	75.00	53.00	23.00	
Sr	346.00	706.00	1494.00	1231.00	957.00	887.00	1345.20	802.00	481.00	464.90	624.00	685.00	637.00	478.00	470.00	419.00	496.00	402.00	
Zr	165.00	184.00	246.00	211.00	243.00	118.00	126.00	175.00	154.00	103.00	129.00	203.00	183.00	195.00	193.00	173.00	202.00	156.00	
Nb	8.10	12.20	11.80	12.50	9.90	14.00	16.00	8.20	6.80	11.00	9.00	11.90	9.20	10.90	10.70	10.00	8.90	8.20	
La	28.20	15.50	35.30	37.50	32.10	27.40	22.10	33.70	27.40	16.30	10.60	34.50	39.90	31.50	30.90	32.70	26.70	25.00	
Ce	59.40	24.20	69.90	74.60	66.70	62.30	49.00	61.60	48.30	33.00	23.40	70.10	76.70	62.70	61.30	64.20	56.80	50.50	
Pr	6.84	3.21	8.27	8.95	7.64	6.24	5.20	6.98	5.79	4.13	2.56	8.44	8.56	7.44	7.25	7.52	6.79	5.92	
Nd	26.60	11.10	28.20	31.10	30.80	22.20	21.80	26.90	22.70	16.50	12.20	29.50	33.50	25.70	25.30	26.00	26.90	20.70	
Sm	4.78	2.41	5.12	5.75	5.39	4.50	3.60	4.77	4.22	3.00	2.40	5.79	5.82	5.00	4.88	4.80	5.22	4.19	
Eu	1.38	0.79	1.40	1.74	1.47	1.15	0.90	1.31	1.21	1.39	0.94	1.70	1.65	1.42	1.40	1.35	1.40	1.24	
Gd	3.15	1.89	3.33	3.69	3.84	3.79	3.49	3.50	3.07	2.95	2.48	4.29	4.04	3.49	3.33	3.20	3.67	3.16	
Tb	0.40	0.29	0.44	0.48	0.48	0.52	0.50	0.46	0.41	0.37	0.32	0.60	0.54	0.45	0.43	0.42	0.46	0.46	
Dy	1.89	1.58	2.05	2.21	2.10	2.53	2.45	2.29	2.08	1.78	1.65	3.06	2.53	2.05	1.89	1.94	2.10	2.39	
Ho	0.33	0.30	0.33	0.35	0.34	0.40	0.35	0.40	0.36	0.28	0.24	0.53	0.44	0.33	0.30	0.32	0.35	0.43	
Er	0.87	0.83	0.82	0.91	0.88	1.17	0.89	1.07	0.97	0.84	0.72	1.41	1.17	0.82	0.76	0.82	0.87	1.17	
Tm	0.12	0.12	0.11	0.13	0.12	0.16	0.11	0.16	0.13	0.08	0.08	0.20	0.16	0.11	0.11	0.11	0.12	0.17	
Yb	0.79	0.79	0.73	0.78	0.76	1.20	1.10	0.98	0.80	0.70	0.70	1.17	1.05	0.67	0.66	0.70	0.73	1.10	
Lu	0.13	0.12	0.11	0.12	0.12	0.17	0.15	0.16	0.12	0.10	0.12	0.17	0.17	0.10	0.10	0.11	0.11	0.17	
Y	8.80	8.70	10.50	11.00	9.20	12.20	10.90	11.80	10.60	8.20	6.70	17.20	12.00	10.30	9.70	10.00	9.10	13.10	
Cs	1.30	7.20	8.00	4.50	4.60	6.30	1.30	7.10	15.60	1.70	1.00	9.30	4.80	8.50	5.60	6.00	3.40	6.70	
Ta	0.46	0.71	0.63	0.62	0.52	–	–	0.65	0.52	–	–	0.63	0.54	0.57	0.58	0.56	0.48	0.46	
Hf	4.10	5.10	6.00	5.40	5.80	3.00	2.00	4.40	3.80	3.00	3.00	5.20	4.50	5.00	4.90	4.60	4.70	4.00	
V	52.00	70.00	58.00	83.00	60.00	103.00	110.00	77.00	56.00	96.00	102.00	88.00	66.00	61.00	63.00	72.00	64.00	100.00	
Ga	21.00	23.00	23.00	26.00	21.00	19.00	24.00	23.00	21.00	21.00	22.00	22.00	22.00	22.00	23.00	22.00	22.00	19.00	
Ge	1.20	1.20	1.40	1.20	1.30	1.00	1.00	1.10	1.00	2.00	–	1.30	0.90	1.10	1.20	0.90	1.20	1.00	
W	0.00	1.50	0.70	0.70	0.00	14.00	453.00	–	–	23.00	46.00	1.10	0.70	0.60	1.00	0.80	0.00	1.10	
Tl	0.27	0.33	0.10	0.24	0.25	0.50	–	0.53	0.51	0.50	–	0.36	0.63	0.45	0.49	0.82	0.58	0.10	
Th	4.11	4.74	4.36	3.92	4.46	7.60	5.50	7.15	4.73	4.20	4.40	4.12	5.03	3.67	3.74	4.02	5.01	3.74	
U	1.24	4.44	2.35	1.83	1.29	2.50	1.60	2.93	1.77	1.50	1.70	2.39	4.86	1.48	1.91	1.45	1.41	3.47	
Sc	4.00	6.00	4.00	6.00	4.00	52.70	85.60	6.00	4.00	53.70	46.90	7.00	5.00	4.00	4.00	5.00	4.00	8.00	
Cr	<20	<20	<20	<20	<20	266.00	188.00	50.00	<20	237.00	214.00	<20	<20	<20	<20	<20	<20	20.00	
Co	<1	1.00	7.00	10.00	7.00	11.00	7.20	10.00	5.00	8.00	2.70	7.00	4.00	7.00	7.00	7.00	2.00	13.00	
Ni	<20	<20	<20	<20	<20	14.00	14.00	<20	<20	15.00	17.00	<20	<20	<20	<20	<20	<20	<20	
La/Yb	35.70	19.62	48.36	48.08	42.24	22.83	20.09	34.39	34.25	23.29	15.14	29.49	38.00	47.01	46.82	46.71	36.58	22.73	
Sm/Yb	6.05	3.05	7.01	7.37	7.09	3.75	3.27	4.87	5.28	4.29	3.43	4.95	5.54	7.46	7.39	6.86	7.15	3.81	
Eu/*Eu	1.09	1.13	1.04	1.16	0.99	0.85	0.78	0.98	1.03	1.43	1.18	1.04	1.04	1.04	1.06	1.05	0.98	1.04	
$(La/Sr)_N$	0.73	0.20	0.21	0.27	0.30	0.28	0.15	0.38	0.51	0.32	0.15	0.45	0.56	0.59	0.59	0.70	0.48	0.56	
$(La/Yb)_N$	12.14	6.67	16.44	16.35	14.36	7.76	6.83	11.69	11.65	7.92	5.15	10.03	12.92	15.99	15.92	15.88	12.44	7.73	
ASI	0.74	1.16	0.94	0.93	0.97	0.85	0.71	0.89	0.91	1.04	0.76	0.80	0.90	0.78	0.89	0.96	0.93	0.83	

Table 2 (*Continued*)

Mineralized areas										
San Pedro Porphyry		Infiernillo porphyry								
CMC	Upper section		Lower section							Upper section
Stratigraphic Unit	Quebrada del Pimiento F.	Cerro Carrizalito F.	Cochicó Group							Quebrada del Pimiento F.
Lithology	Basanite	Rhyolitic tuff	Dacitic Tuff	Dacitic Tuff	Dacitic Tuff	Dacitic Tuff	Dacitic Tuff	Dacitic Tuff	Dacite	Andesite
Samples	LP4†	CSP1085†	146/06	M11	M13	INF4	INF6	M39	INF7	M44D
Latitude S	35°21′43.39″S	35° 23.203″ S	34°39.605′	34°38.720′	34°38.720′	34° 38.086′	34° 38.739	34°39.136′	34°37.761′	34°38.860
Longitude W	68°23′3.56″O	68 24.286″O	68°47.977	68°47.091′	68°47.144′	68° 47.594′	68° 47.185	68°47.206	68°47.438	68°48.574
SiO_2	50.21	76.33	65.70	68.8	69.11	69.6	69.4	69.34	67.3	–
TiO_2	0.67	0.11	0.40	0.363	0.383	0.4	0.5	0.379	0.5	–
Al_2O_3	13.35	12.16	13.80	14.14	15.30	14.40	14.60	14.77	14.40	–
FeO	–	–	–	–	–	–	–	–	–	–
Fe_2O_3	6.67	2.01	2.41	2.70	2.94	2.24	2.54	2.86	3.28	–
MnO	0.12	0.05	0.30	0.11	0.10	0.01	0.05	0.10	0.02	–
MgO	4.47	0.34	0.40	0.39	0.30	0.30	0.30	0.31	0.50	–
CaO	8.90	0.29	4.20	3.30	1.46	2.80	2.80	1.83	2.70	–
Na_2O	2.57	2.89	2.00	2.67	3.01	3.40	3.30	2.62	3.00	–
K_2O	1.59	4.71	3.70	3.05	3.82	3.70	2.80	3.79	4.00	–
P_2O_5	0.19	–	0.15	0.15	0.19	0.15	0.15	0.15	0.15	–
LOI	10.54	1.47	5.80	4736.00	3048.00	2.70	3.20	3.52	4.30	–
Ba	670.00	290.00	373.00	745.00	943.00	877.00	1090.00	1109.00	1680.00	473.00
Rb	29.00	160.00	152.00	120.00	122.00	80.00	91.00	120.00	147.00	135.00
Sr	846.00	68.00	128.00	315.00	244.00	311.00	518.00	287.00	436.00	861.00
Zr	135.00	114.00	152.00	139.00	143.00	157.00	151.00	133.00	165.00	161.00
Nb	4.60	11.10	6.30	7.00	7.00	7.60	7.20	7.00	7.90	6.60
La	24.40	16.80	32.20	29.50	30.00	28.60	28.50	30.00	29.20	25.30
Ce	50.70	43.00	61.80	62.30	63.10	56.20	56.30	62.00	57.30	52.70
Pr	6.17	5.09	7.55	6.98	7.02	6.56	6.59	7.02	6.72	6.80
Nd	24.90	19.90	29.00	26.10	26.30	25.10	25.60	26.50	25.80	24.20
Sm	4.96	4.95	4.90	4.50	4.40	4.46	4.66	4.50	4.53	5.25
Eu	1.26	0.30	1.38	1.26	1.22	1.18	1.26	1.37	1.22	1.39
Gd	3.84	4.52	3.35	3.10	3.20	3.31	3.36	3.50	3.32	4.60
Tb	0.58	0.81	0.47	0.40	0.40	0.45	0.46	0.50	0.47	0.68
Dy	3.27	5.08	2.22	2.10	2.10	2.19	2.10	2.30	2.18	3.77
Ho	0.62	1.01	0.40	0.40	0.40	0.39	0.37	0.40	0.39	0.75
Er	1.82	2.99	1.11	1.00	1.00	1.11	1.05	1.10	1.07	2.26
Tm	0.27	0.49	0.16	0.15	0.15	0.16	0.15	0.16	0.16	0.33
Yb	1.70	3.09	1.00	1.00	0.90	1.01	0.98	1.00	1.02	2.09
Lu	0.25	0.46	0.15	0.15	0.15	0.15	0.14	0.15	0.15	0.31
Y	17.40	28.30	11.20	10.00	11.00	11.40	11.30	12.00	11.90	22.20
Cs	1.60	5.20	9.40	11.20	8.00	–	–	9.30	–	26.20
Ta	0.28	1.24	0.58	0.60	0.70	0.67	0.62	0.60	0.66	0.41
Hf	3.20	3.90	4.30	4.00	3.90	4.20	4.00	3.70	4.50	4.20
V	159.00	12.00	39.00	40.00	40.00	–	–	41.00	–	148.00
Ga	17.00	15.00	23.00	23.00	23.00	–	–	22.00	–	17.00
Ge	1.10	1.20	1.50	1.00	2.00	–	–	1.00	–	1.00
W	–	0.60	3.20	< 1	< 1	–	–	< 1	–	38.60
Tl	0.13	0.91	2.19	1.10	1.30	–	–	1.40	–	2.24
Th	4.37	14.90	5.75	6.60	7.60	7.35	6.19	6.70	6.74	3.69
U	1.75	4.41	2.45	6.30	2.10	–	–	2.50	–	1.29
Sc	21.00	6.00	–	4.00	5.00	–	–	5.00	–	–
Cr	280.00	<20	–	50.00	<20	–	–	50.00	–	–
Co	27.00	2.00	–	5.00	5.00	–	–	2.00	–	–
Ni	90.00	<20	–	<20	<20	–	–	<20	–	–
La/Yb	14.35	5.44	32.20	29.50	33.33	28.32	29.08	30.00	28.63	12.11
Sm/Yb	2.92	1.60	4.90	4.50	4.89	4.42	4.76	4.50	4.44	2.51
Eu/*Eu	0.88	0.20	1.04	1.03	0.99	0.94	0.97	1.06	0.96	0.86
$(La/Sr)_N$	0.26	2.22	2.26	0.84	1.11	0.83	0.50	0.94	0.60	0.26
$(La/Yb)_N$	4.88	1.85	10.95	10.03	11.33	9.63	9.89	10.20	9.73	4.12
ASI	0.60	1.17	0.92	1.03	1.30	0.98	1.08	1.26	1.02	NaN

Table 2 (*Continued*)

Mineralized areas									
San Pedro Porphyry	Arroyo La Chilca - Zanjón del Buitre porphyry					Don Sixto			
CMC	Lower section					Upper section			
Stratigraphic Unit	Cochicó Group					Choique Mahuida F.		El Portillo Group	
Lithology	Dacite Dyke	Andesite	Dacitic Tuff	Dacitic Tuff	Dacitic Tuff	Rhyolite	Rhyolite	Rhyolite	Rhyolite
Samples	LCH5	LCH10	86010	86015	86017	CM101	CM106	EP82	EP104
Latitude S	35° 25′28.2″	35° 25′28.7″	35°25.450′	35°.25.430′	35°25.110	36°17′49.4″	36°17′59.8″	36°17′29.4″	36°17′50.5″
Longitude W	68° 20′8.1″	68° 19′58.8″	68°19.944′	68°19.731	68°19.209	68°27′24.4″	68°27′17.8″	68°27′27.9″	68°27′20.8″
SiO_2	62.46	60.03	–	–	–	77.19	77.55	78.03	78.81
TiO_2	0.48	0.66	0.55	0.17	0.18	0.18	0.09	0.08	0.09
Al_2O_3	14.70	16.26	–	–	–	13.63	12.22	12.00	12.56
FeO	–	–	–	–	–	1.10	0.88	0.88	0.33
Fe_2O_3	3.95	4.65	–	–	–	0.55	0.44	0.44	0.17
MnO	0.10	0.09	–	–	–	0.01	0.03	0.02	0.01
MgO	1.62	1.38	–	–	–	0.14	0.04	0.07	0.07
CaO	3.82	4.04	–	–	–	0.17	0.64	0.58	0.24
Na_2O	3.37	3.01	–	–	–	1.52	3.21	3.90	4.97
K_2O	3.50	3.09	2.66	3.17	2.99	5.47	4.88	3.97	2.73
P_2O_5	0.20	0.27	0.17	0.11	0.17	0.04	0.02	0.02	0.03
LOI	4.80	6.26	–	–	–	1.94	0.92	1.20	0.95
Ba	4722.00	1171.00	2810.00	1850.00	1040.00	762.00	84.00	159.00	216.00
Rb	99.00	104.00	120.00	115.00	64.00	173.00	149.00	164.00	115.00
Sr	583.00	479.00	524.00	374.00	453.00	39.00	21.00	28.00	57.00
Zr	141.00	213.00	–	–	–	253.00	164.00	155.00	173.00
Nb	7.60	10.30	–	–	–	14.00	15.00	28.00	27.00
La	29.00	31.70	34.00	27.80	27.30	38.30	35.80	34.00	33.90
Ce	52.30	64.00	72.00	57.00	54.00	50.60	82.40	81.10	68.10
Pr	5.88	7.67	–	–	–	8.02	9.82	10.10	9.68
Nd	22.40	30.40	–	–	–	29.90	36.20	38.00	36.30
Sm	3.94	5.44	6.00	3.40	3.70	5.10	8.60	10.70	9.90
Eu	1.06	1.46	1.50	0.60	0.90	0.29	0.16	0.15	0.22
Gd	2.83	3.62	–	–	–	3.80	6.80	8.90	8.10
Tb	0.39	0.43	–	–	0.90	0.70	1.30	2.00	1.80
Dy	2.11	1.99	–	–	–	4.60	7.70	11.70	10.20
Ho	0.38	0.29	–	–	–	1.00	1.60	2.50	2.10
Er	1.07	0.73	–	–	–	3.10	4.50	7.00	6.10
Tm	0.16	0.09	–	–	–	0.54	0.76	1.21	1.06
Yb	1.05	0.52	0.80	1.00	0.40	3.40	4.60	7.40	6.30
Lu	0.16	0.07	0.31	0.13	0.08	0.52	0.65	1.04	0.88
Y	11.40	8.20	10.00	11.60	7.30	29.00	41.00	66.00	55.00
Cs	5.00	7.90	12.00	–	–	29.00	41.00	66.00	55.00
Ta	0.62	0.69	0.60	–	–	1.20	1.40	2.80	2.60
Hf	3.50	4.90	5.00	3.00	5.00	7.40	6.10	7.20	7.20
V	72.00	74.00	97.00	47.00	53.00	–	–	–	–
Ga	20.00	24.00	–	–	–	18.00	17.00	20.00	21.00
Ge	1.10	1.00	–	–	–	–	–	–	–
W	–	–	35.00	117.00	59.02	–	–	–	–
Tl	0.80	1.08				0.80	0.40	0.80	1.00
Th	6.67	4.40	2.50	7.60	5.90	18.40	17.60	30.00	28.00
U	2.76	1.24	1.70	3.60	6.50	3.70	5.10	9.50	6.60
Sc	6.00	5.00	–	–	–	–	–	–	–
Cr	<20	20.00	–	–	–	10.00	10.00	10.00	10.00
Co	9.00	9.00	–	–	–	37.00	83.00	146.00	145.00
Ni	<20	<20	–	–	–	10.00	10.00	10.00	10.00
La/Yb	27.62	60.96	42.50	27.80	68.25	11.26	7.78	4.59	5.38
Sm/Yb	3.75	10.46	7.50	3.40	9.25	1.50	1.87	1.45	1.57
Eu/*Eu	0.97	1.01	–	–	–	0.20	0.06	0.05	0.08
$(La/Sr)_N$	0.45	0.60	0.58	0.67	0.54	8.84	15.34	10.93	5.35
$(La/Yb)_N$	9.39	20.73	14.45	9.45	23.21	3.83	2.65	1.56	1.83
ASI	0.90	1.04	0.00	0.00	0.00	1.56	1.04	1.02	1.09

Table 2 (*Continued*)

Unmineralized areas San Rafael Massif										
CMC	Lower section									
Stratigraphic Unit	Cochicó Group									
Lithology	Andesite	Tuff	Tuff	Andesitic breccia	Tuff	Tuff	Tuff	Tuff	Tuff	Tuff
Samples	LCA1	LCA2	LCI1	LCI2	LCI4	LCI5	LCI6	LCI7	LCI8	77/90
Latitude S Longitude W	Unspecified	Unspecified	Unspecified	Unspecified	Unspecified	Unspecified	Unspecified	Unspecified	Unspecified	Unspecified
SiO_2	63.24	59.11	63.70	66.37	67.80	68.43	68.59	69.71	67.09	70.04
TiO_2	0.73	0.83	0.50	0.43	0.50	0.34	0.30	0.45	0.49	0.38
Al_2O_3	16.73	17.28	15.40	14.98	15.74	15.33	15.01	14.47	15.94	15.68
FeO	2.20	1.04	0.87	0.15	0.18	0.31	0.20	0.22	0.49	0.24
Fe_2O_3	1.76	6.08	2.67	2.91	3.20	2.29	2.65	2.55	2.44	2.14
MnO	0.07	0.13	0.06	0.04	0.06	0.02	0.05	0.06	0.05	0.03
MgO	1.30	1.72	1.24	0.90	0.73	0.67	1.00	0.26	0.78	0.85
CaO	3.20	4.52	3.64	2.50	2.60	2.08	1.33	2.54	2.43	2.14
Na_2O	3.35	4.09	3.22	4.05	3.39	4.89	4.38	3.83	4.03	2.75
K_2O	3.36	2.91	2.46	3.55	3.79	2.91	3.28	2.98	3.46	4.18
P_2O_5	0.22	0.37	0.13	0.18	0.20	0.09	0.15	0.10	0.14	0.13
LOI	3.85	1.92	2.21	2.60	2.00	2.85	2.35	2.88	2.28	1.44
Ba	875.00	1271.00	626.00	1070.00	1439.00	1256.00	1302.00	852.00	1055.00	980.00
Rb	120.00	66.00	101.00	93.00	133.00	81.00	97.00	82.00	105.00	122.00
Sr	460.00	904.00	495.00	688.00	708.00	723.00	776.00	691.00	665.00	540.00
Zr	183.00	182.00	90.00	75.00	80.00	75.00	65.00	84.00	92.00	98.00
Nb	13.00	11.00	13.00	2.00	6.00	11.00	7.00	5.00	–	11.00
La	34.90	31.00	29.30	25.90	27.20	27.80	26.60	26.20	28.60	26.75
Ce	70.10	70.20	56.90	51.90	57.70	54.30	53.50	52.00	57.50	56.24
Pr	–	–	7.81	–	–	–	–	–	–	–
Nd	33.60	34.30	27.60	27.00	27.40	26.80	25.70	25.80	29.30	22.97
Sm	6.88	6.42	5.32	5.02	5.28	5.06	4.85	4.72	5.37	3.61
Eu	1.40	1.77	1.48	1.29	1.28	1.18	1.37	1.21	1.40	0.99
Gd	6.44	5.44	4.24	3.70	4.09	3.69	3.41	3.28	3.92	3.06
Tb	–	–	0.59	–	–	–	–	–	–	–
Dy	5.27	4.09	2.54	2.21	2.60	2.28	2.15	2.07	2.42	1.30
Ho	–	–	0.47	–	–	–	–	–	–	–
Er	2.54	2.13	1.17	1.02	1.18	1.00	1.01	1.03	1.13	0.71
Tm	–	–	0.19	–	–	–	–	–	–	–
Yb	2.70	1.99	1.16	1.00	1.12	1.01	1.02	1.06	1.16	0.61
Lu	0.40	0.30	0.16	0.18	0.18	0.20	0.15	0.15	0.17	0.09
Y	33.00	25.00	15.30	13.20	15.00	13.10	13.30	12.40	14.60	–
Cs	–	–	34.50	–	–	–	–	–	–	–
Ta	–	–	1.17	–	–	–	–	–	–	–
Hf	–	–	4.02	–	–	–	–	–	–	–
V	92.00	121.00	78.00	69.00	74.00	58.00	62.00	58.00	61.00	39.00
Ga	19.00	22.00	24.00	–	–	–	–	–	–	–
Ge	–	–	1.30	–	–	–	–	–	–	–
W	–	–	97.10	–	–	–	–	–	–	–
Tl	–	–	0.61	–	–	–	–	–	–	–
Th	7.00	5.00	8.07	6.51	10.00	6.64	6.65	6.70	7.15	7.00
U	0.90	1.10	1.45	0.35	1.57	1.82	1.04	2.07	1.34	1.40
Sc	–	–	–	–	–	–	–	–	–	4.00
Cr	11.00	12.00	22.00	36.00	26.00	32.00	26.00	33.00	30.00	15.00
Co	55.00	23.00	15.90	–	–	–	–	–	–	–
Ni	7.00	5.00	28.00	–	10.00	–	–	14.00	–	4.00
La/Yb	12.93	15.58	25.26	25.90	24.29	27.52	26.08	24.72	24.66	43.85
Sm/Yb	2.55	3.23	4.59	5.02	4.71	5.01	4.75	4.45	4.63	5.92
Eu/*Eu	0.64	0.92	0.95	0.92	0.84	0.83	1.03	0.94	0.93	0.91
$(La/Sr)_N$	0.68	0.31	0.53	0.34	0.35	0.35	0.31	0.34	0.39	0.45
$(La/Yb)_N$	4.39	5.30	8.59	8.81	8.26	9.36	8.87	8.40	8.38	14.91
ASI	1.12	0.95	1.06	1.00	1.09	1.02	1.14	1.02	1.08	1.21

Table 2 (*Continued*)

Unmineralized areas San Rafael Massif							
CMC	Upper section						
Stratigraphic Unit	Agua de los Burros F.			Quebrada del Pimiento F.		Cerro Carrizalito F.	
Lithology	Tuff	Tuff	Tuff	Andesites	Andesites	Tuff	Tuff
Samples	AB1	AB2	67/88	QP1	QP2	CCI1	CCI2
Latitude S Longitude W	Unspecified	Unspecified	Unspecified	Unspecified	Unspecified	Unspecified	[1,0]Unspecified
SiO_2	71.07	75.94	76.66	60.08	56.70	71.85	76.04
TiO_2	0.41	0.12	0.11	0.94	0.92	0.38	0.12
Al_2O_3	15.26	12.87	13.96	16.99	15.45	13.81	12.30
FeO	0.00	0.06	0.15	4.42	0.00	0.69	1.64
Fe_2O_3	3.28	1.23	1.12	1.18	7.07	2.85	0.95
MnO	0.03	0.02	0.01	0.13	0.10	0.04	0.03
MgO	0.35	0.02	0.05	2.86	3.84	0.10	0.11
CaO	0.52	0.31	0.24	5.96	3.75	1.13	0.72
Na_2O	0.56	4.33	2.02	3.49	3.88	3.13	2.88
K_2O	4.54	4.48	5.30	1.83	2.60	5.48	4.67
P_2O_5	0.11	0.01	0.00	0.22	0.36	0.07	0.02
LOI	3.87	0.61	1.01	1.90	5.32	0.46	0.52
Ba	900.00	181.00	161.00	965.00	1496.00	1080.00	117.00
Rb	197.00	141.00	204.00	115.00	86.00	220.00	148.00
Sr	140.00	18.00	19.00	361.00	1020.00	128.00	37.00
Zr	306.00	141.00	129.00	240.00	209.00	327.00	122.00
Nb	13.10	20.00	16.00	13.00	9.78	15.00	15.00
La	54.60	32.40	28.43	27.60	58.80	51.80	25.80
Ce	112.00	73.40	67.94	63.70	116.00	106.00	60.00
Pr	12.80	8.56	7.61	–	13.70	12.20	–
Nd	46.00	31.20	27.93	28.00	51.20	43.30	30.20
Sm	8.68	6.93	6.14	5.69	9.64	8.43	7.20
Eu	1.45	0.35	0.34	1.47	2.20	1.30	0.50
Gd	7.62	6.68	5.92	5.55	6.98	7.42	6.16
Tb	1.26	1.10	1.02	–	0.99	1.27	–
Dy	6.20	5.54	5.13	4.81	4.50	6.41	5.14
Ho	1.34	1.20	1.09	–	0.91	1.38	–
Er	3.93	3.77	3.47	2.36	2.65	4.31	2.54
Tm	0.62	0.61	0.55	–	0.39	0.66	–
Yb	3.64	3.61	3.34	2.58	2.48	4.13	2.90
Lu	0.53	0.55	0.46	0.38	0.35	0.62	0.42
Y	37.50	36.00	31.80	33.00	26.30	38.90	29.00
Cs	9.42	2.07	6.09	–	10.60	10.90	–
Ta	1.28	1.75	1.43	–	0.64	2.23	–
Hf	8.66	3.78	3.26	–	5.41	8.53	–
V	23.00	–	–	162.00	412.00	–	–
Ga	22.00	18.00	17.00	20.00	24.00	21.00	15.00
Ge	1.70	1.30	1.20	–	1.50	1.50	–
W	153.00	390.00	279.27	–	68.10	662.00	–
Tl	0.79	0.53	1.05	–	0.08	0.86	–
Th	18.40	16.60	15.14	6.00	11.20	20.10	17.00
U	1.80	2.84	5.21	1.50	3.71	3.61	3.30
Sc	–	–	–	–	–	–	–
Cr	–	–	17.00	13.00	43.00	–	11.00
Co	22.10	57.50	31.80	63.00	31.60	81.40	52.00
Ni	14.00	10.00	38.00	13.00	43.00	–	11.00
La/Yb	15.00	8.98	8.51	10.70	23.71	12.54	8.90
Sm/Yb	2.38	1.92	1.84	2.21	3.89	2.04	2.48
Eu/*Eu	0.55	0.16	0.17	0.80	0.82	0.50	0.23
$(La/Sr)_N$	3.51	16.20	13.47	0.69	0.52	3.64	6.28
$(La/Yb)_N$	5.10	3.05	2.89	3.64	8.06	4.26	3.02
ASI	2.25	1.03	1.47	0.92	0.96	1.05	1.11

In the San Pedro, Infiernillo and La Chilca-Zanjón del Buitre porphyries, the rocks were crushes (<7 kg) up to 90% passing 2 mm, riffle spitted (250 g) and pulverized (mild steel) to 95% passing 105 μm including cleaner sand. The major elements and trace elements were analyzed by † inductively coupled plasma/mass spectrometry (ICP-MS code 4LithoResearch) and *ICP e INAA (Neutron Activation Analysis). FeO (0.1%) was analyzed by titration. In the Don Sixto ore deposit major elements (wt%) and trace elements (ppm) were analyzed by ICP in Actlabs. ‡Choique Mahuida F. and El Portillo Group are equivalent to the Cerro Carrizalito F (Mugas Lobos et al., 2010). Major elements and trace elements in rocks from the unmineralized areas were analized by XRF and ICP-MS, Actlabs, Canada. Abbreviations: LOI: Loss ion ignition; ASI: aluminum saturation index; dashed lines: no data available; <20: below the limit of detection.

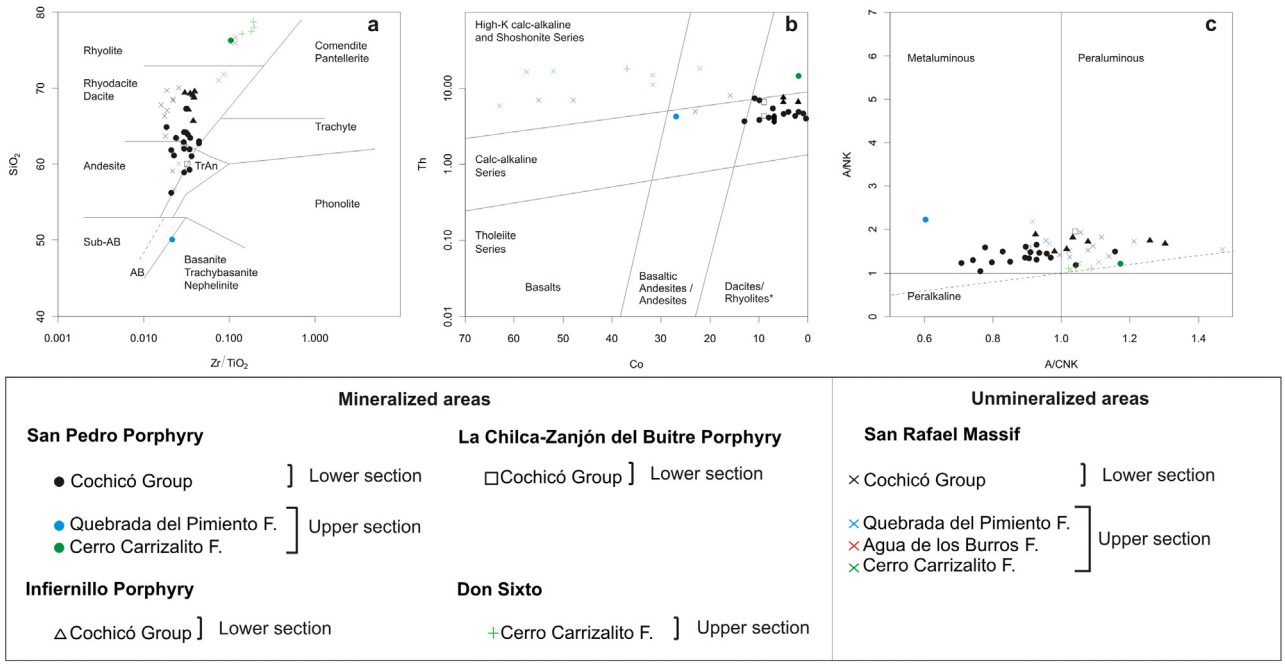

Fig. 4. (a) SiO_2 vs. Zr/TiO_2 classification diagram of volcanic rocks of the CMC (Winchester and Floyd, 1977). (b) Th vs. Co diagram (Hastie et al., 2007). (c) Aluminum saturation index diagram (A/CNK) (Shand, 1943). Abbreviations: TrAn: trachy-andesite; AB: alkali basalt; Sub-AB: sub-alkaline basalt.

such as internal cracks or resorption textures are not observed and the U/Th ratio < 3 is consistent with a magmatic origin (Rubatto, 2002). A total of 30 zircons were analyzed (Table 1) which yielded an age of 263.1 ± 4.2 Ma (Fig. 3). A few older zircons were also found, two of them with ages of ~1.1 and ~1.3 Ga (Grenvillian). Records of Precambrian events of these ages were found in the SRM in Cerro de la Ventana Formation (Cingolani and Varela, 1999). Another inherited core zircon yielded an age of 369.2 ± 8.3 Ma (late Devonian). This age could be correlated with the collision of the Chilenia terrane to the Pacific side of Cuyania terrane (which encompasses the Precordillera, the SRM, the Pie de Palo area and the Las Matras block) by the end of the Devonian (see Ramos et al., 1984; Ramos, 2004; Willner et al., 2008).

On the other hand, three younger zircon analyzes (between 246.7 and 250.1 Ma, see Table 1) are considered as reflecting a lead loss.

5. Geochemical characteristics of the Choiyoi Magmatic Cycle

The samples from SPP area were analyzed in order to characterize the volcanic sequence (Table 2) and compared to other geochemical analyses of representative samples of the lower and upper sections from mineralized and unmineralized zones of the CMC (Kleiman, 1999; Kleiman and Japas, 2009; Gómez and Rubinstein, 2010b; Mugas Lobos et al., 2010; Rubinstein et al., 2012).

According to the SiO_2 versus Zr/TiO_2 diagram (Fig. 4a; Winchester and Floyd, 1977), the Cochicó Group rocks are andesites, trachyandesites and dacites-rhyodacites with a wide range of SiO_2 (59.69–72.12 wt%, in volatile-free basis) and variable contents of Na_2O (2.15–7.83 wt%), K_2O (1.01–4.24 wt%) and Al_2O_3 (14.78–18.29 wt%). These rocks display a calc-alkaline affinity (Fig. 4b; Hastie et al., 2007) and generally show a metaluminous to slightly peraluminous character with an aluminum saturation index (A/CNK) from 0.71 up to 1.1 (Fig. 4c). The rocks with the higher A/CNK (>1.1) belong to phyllic alteration zones. On the other hand, the upper section volcanics from Agua de los Burros and Cerro Carrizalito Formations are predominantly high silica rhyolites (Fig. 4a, SiO_2: 72.19–78.80%wt in volatile-free basis), whereas the Quebrada del Pimiento Formation consists of basanites and andesites (Fig. 4a, SiO_2: 56.58–61.24 wt% in volatile-free basis). All the rocks of the upper section display a high K calc-alkaline affinity (Fig. 4b, Hastie et al., 2007) and are predominantly peraluminous with an A/CNK from 0.6 up to 1.56 (Fig. 4c).

In the Harker diagrams, the rocks of the lower section show an increase in K_2O (Fig. 5h) and a decrease in TiO_2, Fe_2O_3, MgO, CaO and P_2O_5 (Fig. 5a, c, e, f and i) from andesites to rhyolites. Rocks from the upper section only show a very strong decrease in TiO_2, Fe_2O_{3T}, MgO, CaO and P_2O_5, from basalts to rhyolites (Fig. 5a, e, f and i). Both sections do not show any trend for Al_2O_3 and Na_2O (Fig. 5b and g).

The N-MORB normalized trace element patterns from the lower section rocks (Fig. 6a) show a strong relative enrichment in LILE compared with HFSE and a Nb–Ta trough which are common features of calc-alkaline arc magmas. Also, the REE patterns (Fig. 6b) display steep slopes (high La/Yb and moderate to high Sm/Yb ratios) with lack or slightly positive Eu anomalies. These geochemical features suggest that the magma equilibrated with amphibole and garnet-bearing mineral residues. Besides, the high Sr contents together with the absence of negative Eu anomalies indicate that no plagioclase is present in the residue. High La/Yb ratios in addition to low La/Sr ratios and the lack of Eu anomalies confirm the presence of a high pressure phase in the mineral residues (Fig. 6e and f; Kay et al., 1991).

The upper section has normalized trace element patterns similar to that of the lower section but showing a less pronounced Nb–Ta trough (Fig. 6c). On the other hand, the upper section shows relatively flat patterns of REE (medium La/Yb ratios and low Sm/Yb ratios) and negative Eu anomalies indicating plagioclase fractionation (Fig. 6d). The high La/Sr and Eu/Eu* ratios and the relatively low La/Yb ratios suggest evolution of the magma under low pressure conditions in which plagioclase is a stable mineral (Fig. 6e and f; Kay et al., 1991).

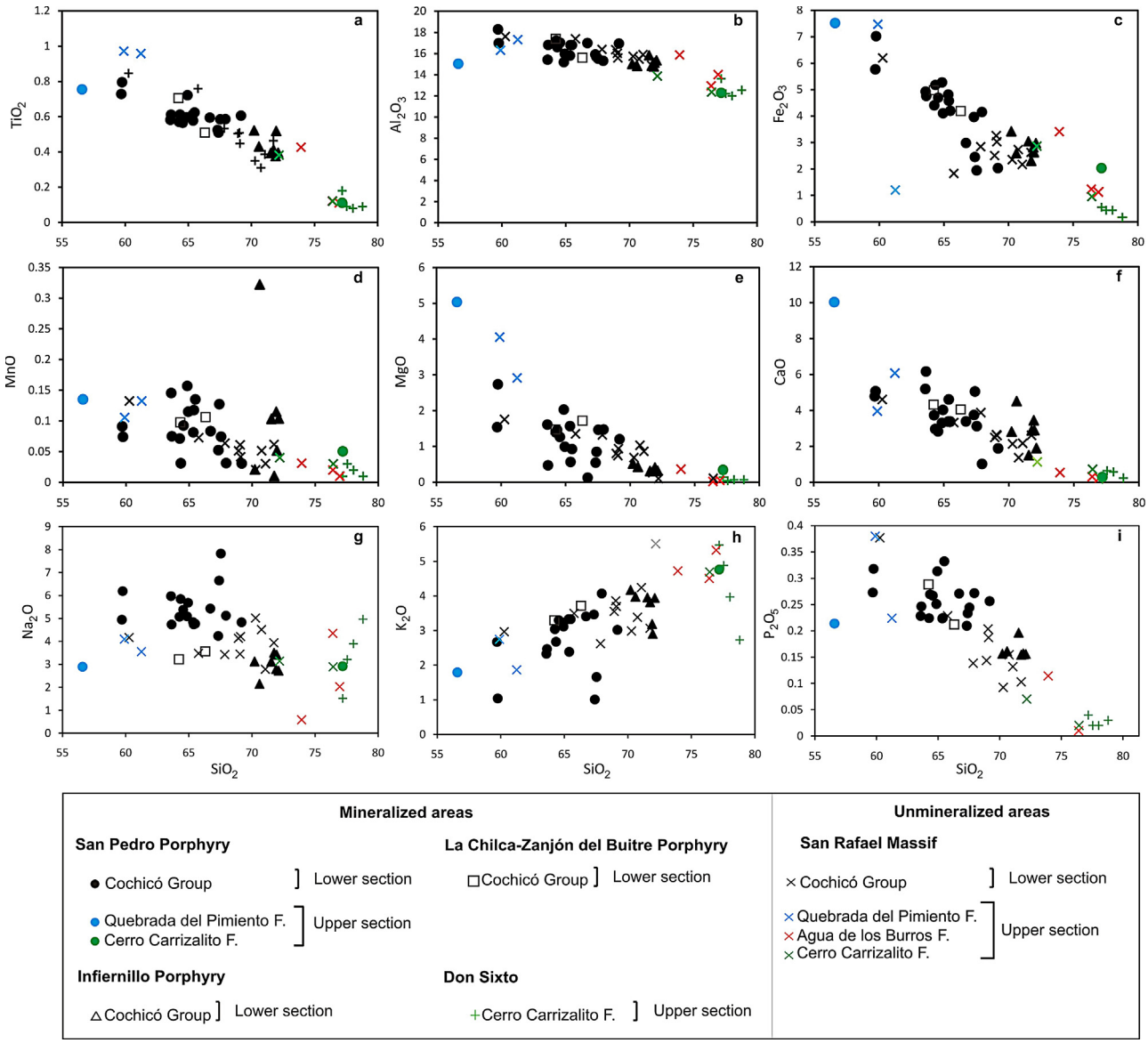

Fig. 5. (a–i) Harker variation diagrams for the CMC volcanics.

6. Discussion

6.1. Adakite-like signature in the CMC

The word adakite was introduced by Defant and Drummond (1990) for intermediate to acidic plutonic and volcanic rocks believed to be products of direct partial melting of subducted oceanic lithosphere at high pressure where garnet is a stable residual phase and plagioclase is absent. The conditions under which the adakites are formed were detailed by Peacock et al. (1994). According to these authors, the necessary geodynamic conditions to allow the formation of adakitic magmas are the subduction of young and hot oceanic plates. More recently, other authors proposed that adakitic rocks can be generated in the presence of an asthenospheric window (Yogodzinski et al., 2001), the partial melting of thickened lower crust (e.g. Atherton and Petford, 1993; Petford and Atherton, 1996) or a delaminated mafic lower crust (e.g. Defant et al., 2002; Xu et al., 2002). However, key adakitic geochemical features (particularly low Y and Yb concentrations and high Sr/Y and La/Yb ratios) can be produced in normal asthenosphere-derived arc magmas by melting-assimilation-storage-homogenization (MASH) and assimilation-fractional-crystallization (AFC) processes (Richards and Kerrich, 2007) which have been well documented particularly in the Central Andes (López, 1982; Kay et al., 1987, 1991; Hildreth and Moorbath, 1988).

Later, Petford and Atherton (1996) found that these geochemical features recognized in the Central Andes are similar to those of adakites considered to be products of slab melting.

Richards and Kerrich (2007) reviewed the link between adakite-like rocks and epithermal- and porphyry-type deposits and concluded that usually the adakitic signature is due to MASH and AFC processes affecting typical arc magmas, predominantly sourced by partial melting of the asthenospheric mantle wedge.

In this paper, we use the word adakite-like to describe rocks with high La/Yb (>9) and Sr/Y (>20) and low Y (≤18 ppm) and Yb (<2 ppm) according to the initial proposal of Defant and Drummond (1990). Based on these criteria, the mineralized subvolcanic and pyroclastic rocks of the CMC lower section from the SRM (San Pedro, Infiernillo and La Chica-Zanjón del Buitre porphyries) show an adakite-like signature. Moreover, in the Y vs. Sr/Y diagram, these rocks plot in the adakitic field just as

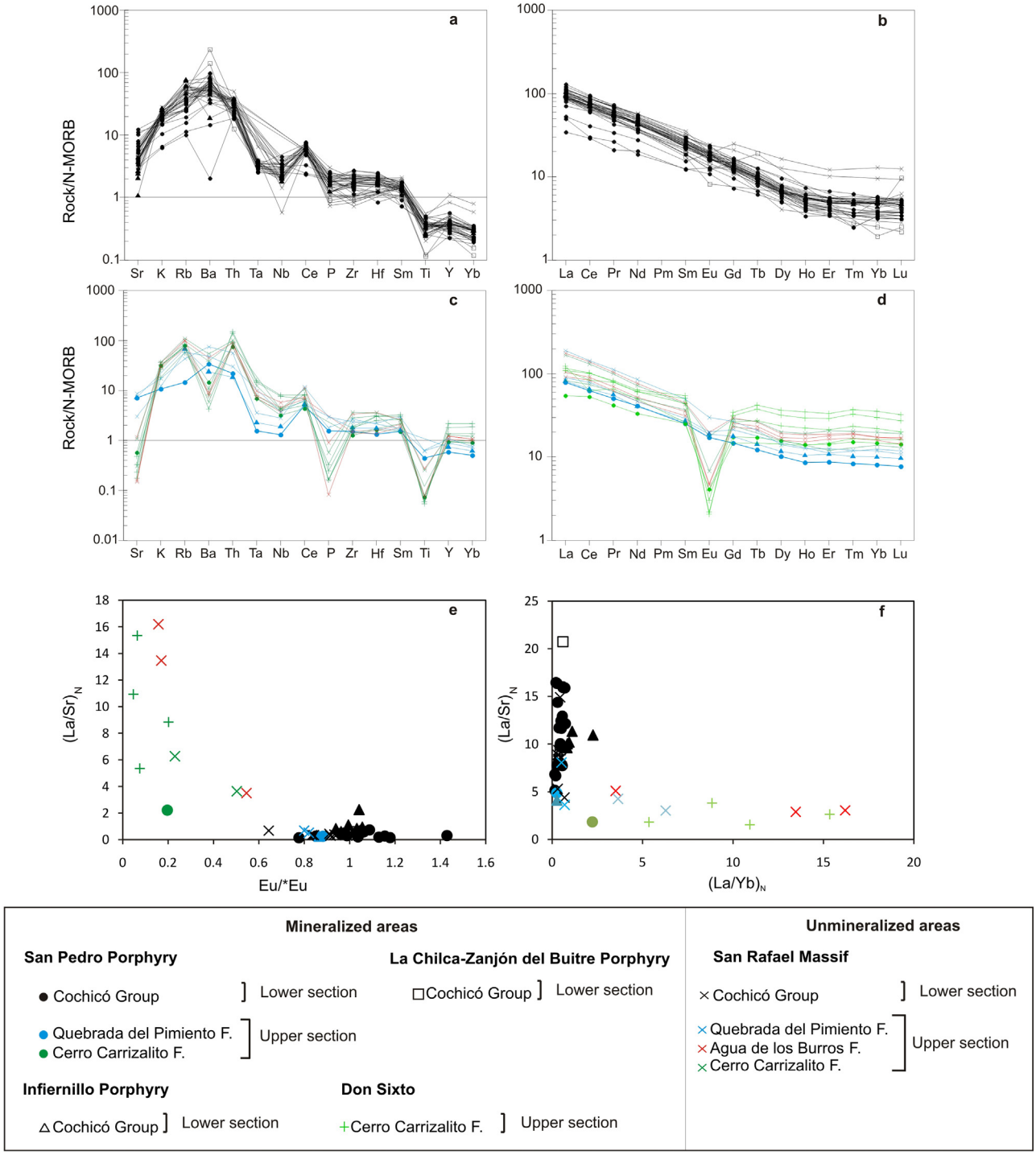

Fig. 6. Spider diagram of the lower (a) and upper (b) section of the CMC volcanics normalized to N-MORB (Pearce, 1983). REE diagram of the lower (c) and upper (d) section normalized to chondrite (Boynton, 1984). $(La/Sr)_N$ vs (Eu/Eu*) (e) and $(La/Sr)_N$ vs. $(La/Yb)_N$ (f) diagrams.

adakite-like rocks genetically linked to Andean porphyry copper deposits (Fig. 7).

6.2. Age of the magmatism related to mineralization

The age obtained for a mineralized sample from the SPP (263.1 ± 4.2 Ma) represents the timing of the CMC lower section arc magmatism genetically linked to the Cu–(Mo) mineralization which is coeval with the age of the Agua de los Burros Formation (264.8 ± 2.3 and 264.5 ± 3.0 Ma; Rocha-Campos et al., 2011) that has a geochemical signature more akin with the upper section of the CMC (see Kleiman and Japas, 2009 and references therein). Therefore, the overlapping of the age ranges of rocks with different geochemical signatures constrains the timing of the emplacement for the San Pedro ore deposit to the transition between a typical subduction setting to a subduction-intraplate transitional setting which is correlated with the change from a transpressive to a transtensive tectonic regime. The link between porphyry type deposits emplacement and the change in the tectonic regime was already proved by Japas et al. (2013) for the Infiernillo ore deposit.

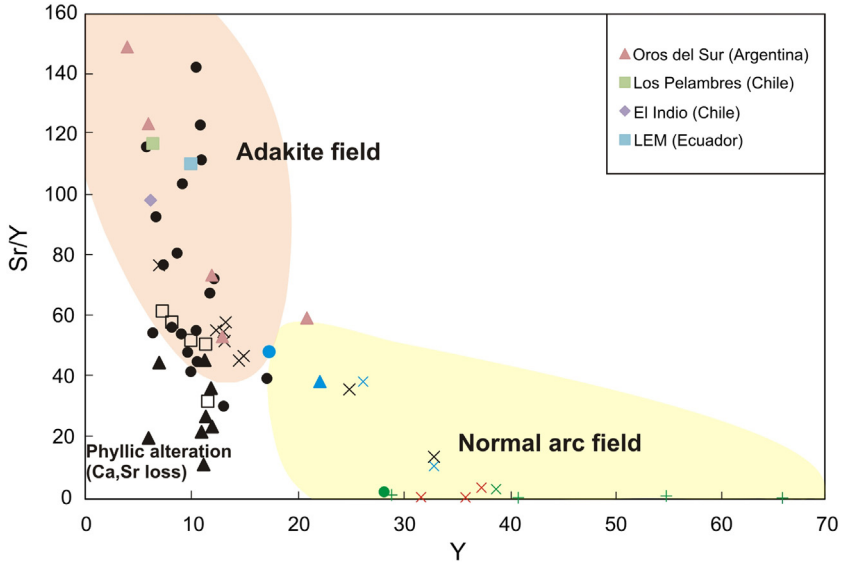

Fig. 7. Sr/Y vs Y diagram (modified from Defant and Drummond, 1990) discriminating normal calcalkaline rocks from adakite-like rocks including adakite-like rocks genetically linked to the porphyry copper and epithermal deposits of Los Pelambres (Reich et al., 2003), El Indio (Bissig et al., 2003), Oro del Sur (Carrasquero et al., 2011) and mineralized LEM volcanics from Ecuador (Chiaradia et al., 2004). See Fig. 6 for references of the CMC volcanics.

6.3. Geochemical evolution of the CMC and petrogenetic implications

The contrasted geochemical signatures recorded in the upper and lower sections of the CMC are linked to the geodynamic evolution of the SRM. According to Kleiman and Japas (2009) during the Early to Mid Permian (~280–265 Ma), the onset of arc-related rocks of the lower section was coeval with the transpressional movements associated with the SRO. The magmatic composition and the inland expansion of the lower section volcanics, as well as the kinematics of structures, reveal a shallowing of the slab at the SRM latitude (Kleiman and Japas, 2009). The end of subduction and subsequent gravitational collapse of the oceanic plate together with the extensional collapse of the orogen resulted in the development of the upper section volcanism by the Mid to Late Permian (~263–251 Ma; Kleiman and Japas, 2009).

The lower section volcanics (composed of intermediate to acidic calc-alkaline lavas and tuffs) display a dominant adakite-like signature. Moreover, the moderate to high Sm/Yb ratios suggests that the mineral residue changed from amphibole to garnet (Fig. 8) which would be consistent with crustal thickening related to a progressive slab shallowing as proposed by Kleiman and Japas (2009) for the Lower Permian in the SRM. This geodynamic setting could favor AFC and MASH processes at higher pressure, which could be responsible for the CMC lower section adakite-like signature.

The upper section volcanics (composed of acidic lavas and tuffs and basaltic-andesitic dykes) differ from those of the lower section by their lack of any adakitic signature. The spider diagram (Fig. 6c) shows a decrease in the subduction signature from the lower to the upper section volcanics, suggesting a transition between a subduction-related calc-alkaline suite and a mildly alkaline suite indicative of an intraplate setting (Kleiman and Japas, 2009). The REE diagram (Fig. 6d) displays a flat pattern for the HREE and exhibit negative Eu-anomalies. These characteristics suggest that the magmas evolved under conditions of plagioclase stability consistent

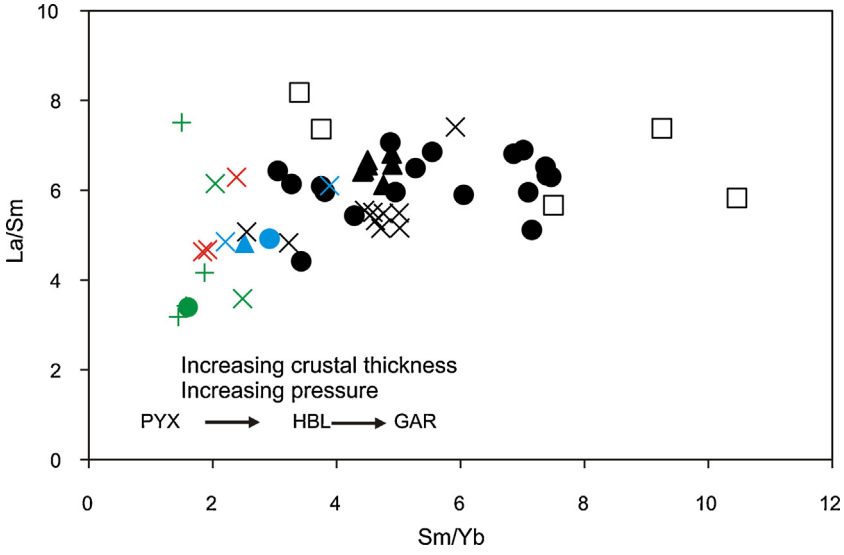

Fig. 8. Sm/Yb vs. La/Yb diagram for the CMC volcanics. See Fig. 6 for references.

with a normal thickness crust (Fig. 8; Kay et al., 1991; Kay and Mpodozis, 2001).

7. Conclusions

The tecto-magmatic evolution of the San Rafael Massif provides an important key to understanding the mineralizing potential of the Gondwanan magmatism. The petrogenetic analysis of the Choyoi Magmatic Cycle arc magmatism genetically linked to the Permian porphyry copper deposits reveal an adakite-like signature which would have acquired in a flat slab geodynamic setting. Moreover, the age of the San Pedro porphyry deposit (~263 Ma) is within the range of the age proposed for the tectonic regime change, confirming that the genesis of the porphyry copper deposits of the San Rafael Massif took place during the waning of the San Rafael Orogeny.

Because of the metallogenic significance of rocks with adakite-like signature, geochemical characterization of such magmatism could result in a powerful tool during the initial stages of ore deposit exploration in the San Rafael Massif.

Acknowledgments

The authors wish to thank H. Malimacci and the Servicio Geológico Minero de Argentina (SEGEMAR) for their support during the fieldwork. This research was funded by UBA-CyT 20020090100182 (Universidad de Buenos Aires) and PIP 11220090100589 (CONICET) projects.

References

Atherton, M.P., Petford, N., 1993. Generation of sodium-rich magmas from newly underplated basaltic crust. Nature 362, 144–146.
Bermúdez, A., Delpino, D., Frey, F., Saal, A., 1993. Los basaltos de retroarco extraandinos. In: Ramos, V.A. (Ed.), Geología y recursos naturales de Mendoza, 12° Congreso Geológico Argentino y 2° Congreso de Exploración e Hidrocarburos, vol. 1. Relatorio, Mendoza, pp. 161–172.
Bissig, T., Clark, A., Lee, K.W., Von Quadt, A., 2003. Petrogenetic and metallogenetic responses to Miocene slab flattening: new constraints from the El Indio-Pascua Au–Ag–Cu Belt. Chile/Argentina Miner. Deposita 38, 844–862.
Bordonaro, O., Keller, M., Lehnert, O., 1996. El Ordovícico de Ponón-Trehue en la provincia de Mendoza (Argentina): Redefiniciones estratigráficas. XIII Congreso Geológico Argentino y 3° Congreso Exploración de Hidrocarburos, Vol. 1. Actas, Buenos Aires, pp. 541–550.
Boynton, W.V., 1984. Consmochemistry of the rare earth elements meteorite studies. In: Henderson, P. (Ed.), Rare Earth Element Geochemistry. Elsevier Sciences, Amsterdam, pp. 63–114.
Bray Du, E.A., Ludington, S., Brooks, W.E., Gamble, B.M., Ratte, J.C., Richter, D.H., Soria Escalante, E., 1995. Compositional characteristics of middle to upper Tertiary volcanic rocks of the Bolivian Altiplano. U.S. Geol. Surv. Bull. 2119, 1–41.
Carpio, F., Mallimacci, H., Rubinstein, N., Salvarredi, J., Sepúlveda, E., Centeno, R., Rosas, M., Vargas, D., 2001. Metalogenia del Bloque de San Rafael, Mendoza. Servicio Geológico Minero Argentino, Serie Contribuciones Técnicas. Recursos Miner. 20, 1–109.
Carrasquero, S., Rubinstein, N., Fontignie, D., 2011. Adakitic-like signature in volcanic rocks associated to Oro Del Sur ore deposit, southern Precordillera, Argentina. Neues Jahrbuch für Geologie und Paläontologie - Abhandlungen, 261 3, 309–320.
Chang, Z., Vervoort, J.D., Mcclelland, W.C., Knaack, C., 2006. U-Pb dating of zircon by LA-ICP-MS. Geochem. Geophys. Geosyst. Q05009, 7, http://dx.doi.org/10.1029/2005GC001100.
Chiaradia, M., Fontboté, L., Beate, B., 2004. Cenozoic continental arc magmatism and associated mineralization in Ecuador. Miner. Dep. 39, 204–222.
Cingolani, C.A., Varela, R., 1999. Rb–Sr isotopic age of the basement rocks of the San Rafael Block, Mendoza, Argentina. II South American Symposium on Isotope Geology, Carlos Paz. Extend. Abstr., 23–26.
Coldwell, B., Petford, N., Murphy, P., Smith, M., 2005. Adakitic rocks of the Yungay Formation, Peru: problems with tectonic setting and origin. Geophys. Res. Abstr. 7, 02656.
Davicino, R., 2008. A review of the Anchoris project, Mendoza, Argentina. Intern. Rep., 1–39.
Defant, M.J., Drummond, M.S., 1990. Derivation of some modern arc magmas by melting of young subducted oceanic lithosphere. Nature 347, 662–665.
Defant, M.J., Xu, J.F., Kepezhinskas, P., Wang, Q., Zhang, Q., Xiao, L., 2002. Adakites: some variations on a theme. Acta Petrol. Sinica 18, 129–142.
Delpino, D., Pezzutti, N., Godeas, M., Donnari, E., Carullo, M., Núñez, E., 1993. Un cobre porfírico paleozoico superior en el centro volcánico San Pedro, distrito minero el nevado, provincia de Mendoza. C. R. 12, 477–490, ICC–p. 1.
Dessanti, R., 1973. Descripción geológica de la hoja 29d, Bardas Blancas. Provincia de Mendoza. Bol. Serv. Nacl. Minero-Geol. 139, 1–70.
Di Tommaso, I., Rubinstein, N., 2007. Hydrothermal alteration mapping using aster data in Infiernillo porphyry deposit, Argentina. Ore Geol. Rev. 32, 275–290.
Espejo, I.S., López Gamundi, O.R., 1994. Source versus depositional controls on sandstone composition on a foreland basin: El Imperial Formation (mid-Carboniferous-lower Permian) San Rafael Basin, western Argentina. J. Sediment. Res. A64, 8–16.
Fuschini, M., 1968. Informe final Área de Reserva No 26. Infiernillo. Servicio Geológico Minero Argentino, Plan Cordillerano, Zona, pp. 1–33.
Gargiulo, M., Rubinstein, N., Carpio, F., Salvarredi, J., 2007. Caracterización de la zona de alteración central II, Bloque San Rafael, provincia de Mendoza. Rev. Asoc. Geol. Argentina 62, 387–395.
Giambiagi, L., Martinez, A., 2008. Permo-Triassic oblique extension in the Potrerillos Uspallata Area, Western Argentina. J. S. Am. Earth Sci. 26, 252–260.
Gómez, A., 2008. Geología del depósito El Infiernillo, Bloque de San Rafael, Mendoza. Universidad de Buenos Aires, 112 p., Final Work Degree.
Gómez, A., 2013. Caracterización metalogenética del distrito minero San Pedro y su vinculación con el magmatismo gondwánico, Bloque de San Rafael, Mendoza. Universidad de Buenos Aires, pp. 327p, Ph.D. thesis.
Gómez, A., Rubinstein, N., 2010a. Geology of San Pedro mining district, San Rafael Massif, Argentina. Boll. Geofis. Teorica Appl. 51, 236–239.
Gómez, A., Rubinstein, N., 2010b. Caracterización genética del distrito minero El Infiernillo, Bloque de San Rafael, provincia de Mendoza. Rev. Asoc. Geol. Argentina 67, 231–238.
Grégori, D.A., Greco, L.E., Llambías, E., 2003. El intrusivo López Lecube: Evidencias de magmatismo alcalino gondwánico en el sector sudoeste de la provincia de Buenos Aires, Argentina. Rev. Asoc. Geol. Argentina 58, 176–186.
Hastie, A.R., Kerr, A.C., Pearce, J.A., Mitchell, S.F., 2007. Classification of altered volcanic island arc rocks using immobile trace elements: development of the Th Co discrimination diagram. J. Petrol. 48, 2341–2357.
Hildreth, W., Moorbath, S., 1988. Crustal contributions to arc magmatism in the Andes of central Chile. Contrib. Mineral. Petrol. 98, 455–489.
Japas, M.S., Rubinstein, N., Kleiman, A.L.E., 2013. Strain fabric analysis applied to hydrothermal ore deposits emplaced during changing geodynamical conditions (Infiernillo and Las Picazas, San Rafael Massif, Argentina). Ore Geol. Rev. 53, 357–372.
Kay, S.M., Maksaev, V., Moscoso, R., Nasi, C., 1987. Probing the evolving Andean lithosphere: mid-late Tertiary magmatism in Chile (29°–30°30′S) over the modern zone of subhorizontal subduction. J. Geophys. Res. 92 (B7), 6173–6189.
Kay, S.M., Mpodozis, C., Ramos, V., Munizaga, F., 1991. Magma source variations for mid-late Tertiary magmatics rocks associated with a shallowing subduction zone and a thickening crust in the Central Andes (28° to 33°S). In: Harmon, R., Rapela, C.W. (Eds.), Andean Magmatism and Its Tectonic Setting, 265. Geological Society of America Special Paper, pp. 113–137.
Kay, S.M., Mpodozis, C., 2001. Central Andean ore deposits linked to evolving shallow subduction systems and thickening crust. GSA Today 11, 4–9.
Kleiman, L.E., 1999. Mineralogía y petrología del volcanismo permo-triásico y triásico del bloque de San Rafael en el área de Sierra Pintada, provincia de Mendoza y su relación con las mineralizaciones de uranio. Universidad de Buenos Aires, pp. 286p, Ph.D. thesis.
Kleiman, L.E., Japas, M.S., 2009. The Choiyoi volcanic province at 34°S–36°S (San Rafael, Mendoza, Argentina): implications for the late Palaeozoic evolution of the southwestern margin of Gondwana. Tectonophysics 473, 283–299.
Kleiman, L.E., Salvarredi, J.A., 2001. Petrología, geoquímica e implicancias tectónicas del volcanismo Triásico (Formación Puesto Viejo), Bloque San Rafael, Mendoza. Rev. Asoc. Geol. Arg. 56, 559–570.
Linares, E., 2007. Catálogo de edades radimétricas de la República Argentina. Años 1957-2005. Asoc. Geol. Argentina, Ser. F, Publ. en CD, 2 (1666-3721).
Llambías, E.J., Sato, A.M., 1995. El Batolito de Colangüil: transición entre orogénesis y anorogénesis. Rev. Asoc. Geol. Argentina 50, 111–131.
Llambías, E.J., Kleiman, L.E., Salvarredi, J.A., 1993. El magmatismo gondwánico. In: Ramos, V.A. (Ed.), Geología y Recursos Naturales de Mendoza y 2° Congreso de Exploración de Hidrocarburos, Vol. 1. Relatorio, Mendoza, pp. 53–64.
Llambías, E.J., Quenardelle, S., Montenegro, T., 2003. The Choiyoi Group from central Argentina: a subalkaline transitional to alkaline association in the craton adjacent to the active margin of the Gondwana continent. J. S. Am. Earth Sci. 16, 243–257.
López, L., 1982. Características geoquímicas de rocas ígneas asociadas con pórfidos cupríferos chilenos. Rev. Geol. Chile 17, 3–19.
Ludwig, K.R., 2003. Isoplot 3.0—Ageochronological toolkit for Microsoft Excel: Special publication No. 4. Berkeley Geochronology Center, Berkeley, Calif, pp. 71 pp.
Mpodozis, C., Kay, S.M., 1992. Late Paleozoic to Triassic evolution of the Gondwana margin: evidence from Chilean Frontal Cordilleran batholiths (28° to 31°S). Geol. Soc. Am. Bull. 104, 999–1014.
Mugas Lobos, A.C., Márquez-Zavalía, M.F., Galliski, M.A., 2010. Petrografía y geoquímica de las rocas gondwánicas del proyecto minero Don Sixto, Mendoza. Rev. Asoc. Geol. Argentina 67, 392–402.

Nasi, C., Mpodozis, C., Cornejo, P., Moscoso, R., Maksaev, V., 1985. El batolito Elqui-Limarí (Paleozoico Superior-Triásico): Características petrográficas, geoquímicas y significado tectónico. Rev. Geol. Chile 24–25, 77–111.

Ottone, E., de la Fuente, M., Monti, M., Naipauer, M., Armstrong, R., Marsicano, C.A., Mancuso, A., 2013. Una edad U/Pb SHRIMP para el Grupo Puesto Viejo y el límite Pérmico- Triásico en el depocentro de San Rafael. In: 5° Simposio Argentino del Paleozoico Superior, Resumenes, Buenos Aires, p. 27.

Paces, J., Miller, J., 1993. Precise U-Pb ages of Duluth complex and related mafic intrusions, northeastern Minnesota; geochronological insights to physical, petrogenetic, paleomagnetic, and tectonomagmatic processes associated with the 1.1 Ga midcontinent rift system. J. Geophys. Res. 98 (B8), http://dx.doi.org/10.1029/93JB01159, ISSN: 0148-0227.

Pearce, J.A., 1983. Role of the sub-continental lithosphere in magma genesis at active continental margins. In: Hawkesworth, C.J., Norry, M.J. (Eds.), Continental Basalts and Mantle Xenoliths. Shiva Publications, Nantwich, Cheshire, pp. 230–249.

Peacock, S., Rushmer, T., Thompson, A.B., 1994. Partial melting of subducting oceanic crust: earth and planetary. Sci. Lett. 121, 227–244.

Petford, N., Atherton, M., 1996. Na-Rich partial melts from newly underplated basaltic crust: the Cordillera Blanca batholith, Peru. J. Petrol. 37, 1491–1521.

Rabbia, O.M., Hernández, L.B., 2000. Quartz diorite trend in porphyry copper deposits: Underlying petrological processes and implications in copper metallogenesis. Mineral. Met. (6), 416–423.

Ramos, V.A., 2004. Cuyania, an exotic block to Gondwana: review of a historical success and the present problems. Gondwana Res. 7, 1009–1026.

Ramos, V.A., Jordan, T., Allmendinger, R., Kay, S., Cortés, J., Palma, M., 1984. Chilenia: un terreno alóctono en la evolución Paleozoica de los Andes Centrales. Actas IX Congreso Geológico Argentino. Actas 2, 84–106.

Ramos, V.A., Munizaga, F., Marín, G., 1988. Las riolitas neopaleozoicas de Sierra de La Huerta (provincia de San Juan): evidencia de una metalogénesis aurífera gondwánica en Sierras Pampeanas. III Congreso Nacional de Geología Económica. Actas 1, 149–159.

Rapela, C.W., Llambías, E.J., 1985. Evolución magmática y relaciones regionales de los complejos eruptivos de La Esperanza, provincia de Río Negro. Rev. Asoc. Geol. Argentina 40, 4–25.

Reich, M., Parada, M.A., Palacios, C., Dietrich, A., Schultz, F., Lehmann, B., 2003. Adakite-like signature of late Miocene intrusions at the Los Pelambres giant porphyry copper deposit in the Andes of central Chile: metallogenic implications. Miner. Deposita 38, 876–885.

Richards, J.P., Kerrich, R., 2007. Adakite-like rocks: their diverse origins and questionable role in metallogenesis. Econ. Geol. 102, 537–576.

Rocha-Campos, A.C., Basei, M.A., Nutman, A.P., Kleiman, L.E., Varela, R., Llambías, E., Canile, F.M., da Rosa, O.C.R., 2011. 30 million years of Permian volcanism recorded in the Choiyoi igneous province (W Argentina) and their source for younger ash fall deposits in the Paraná Basin: SHRIMP U–Pb zircon geochronology evidence. Gondwana Res. 19, 509–523.

Rubatto, D., 2002. Zircon trace element geochemistry: distribution coefficients and the link between U-Pb ages and metamorphism. Chem. Geol. 184, 123–138.

Rubinstein, N., Gargiulo, M.F., 2005. Análisis textural de cuarzo hidrotermal del depósito El Pantanito, provincia de Mendoza: nuevos aportes sobre su génesis. Rev. Asoc. Geol. Argentina 60, 96–103.

Rubinstein, N., Carpio, F., Mallimacci, H., 2002. Las vetas polimetálicas del área del Cerro San Pedro, provincia de Mendoza, Argentina. XV Congreso Geológico Argentino, Calafate: Actas 2, 263–266.

Rubinstein, N.A., Ostera, H., Mallimacci, H., Carpio, F., 2004. Lead isotopes from gondwanan ore polymetallic vein deposits, San Rafael Massif, Argentina. J. S. Am. Earth Sci. 16, 595–602.

Rubinstein, N.A., Gómez, A., Mallimacci, H., 2012. La zona de alteración Arroyo La Chilca–Zanjón del Buitre, Bloque de San Rafael, Mendoza. Rev. Asoc. Geol. Argentina 69, 285–293.

Rubinstein, N., Gómez, A., Kleiman, L., 2013. Caracterización litofacial y geoquímica de las volcanitas del área del distrito minero El Infiernillo, Mendoza. Rev. Asoc. Geol. Argentina 70 (3), 394–401.

Sepúlveda, E., Bermúdez, a., Bordonaro, O. and Delpino, D., Hoja Geológica 3569-IV, Embalse El Nihuil, provincia de Mendoza. Instituto de Geología y Recursos minerales, Servicio Geológico Minero Argentino. Boletín 268. Segunda edición revisada, 2007, 52p.

Shand, S.J., 1943. Eruptive Rocks. Their Genesis, Composition, Classification, and Their Relation to Ore-Deposits with a Chapter on Meteorite. John Wiley & Sons, New York.

Sláma, J., Košler, J., Condon, D.J., Crowley, J.L., Gerdes, A., Hanchar, J.M., Horstwood, M.S.A., Morris, G.A., Nasdala, L., Norberg, N., Schaltegger, U., Schoene, B., Tubrett, M.N., Whitehouse Plešovice, M.J., 2008. Zircon—a new natural reference material for U-Pb and Hf isotopic microanalysis. Chem. Geol. 249 (1–2), 1–35.

Søager, N., Holm, P.M., Llambías, E.J., 2013. Payenia volcanic province, southern Mendoza, Argentina: OIB mantle upwelling in a backarc environment. Chem. Geol. 349–350, 36–53.

Strazzere, L., Gregori, D.A., Dristas, J.A., 2006. Genetic evolution of Permo-Triassic volcaniclastic sequences at Uspallata, Mendoza Precordillera, Argentina. Gondwana Res. 9, 485–499.

Tickyj, H., Tomezzoli, R.N., Basei, M.A., 2014. Primeras edades U-Pb en intrusivos Pérmicos del Distrito Minero Agua Escondida. In: Mendoza XIX Congreso Geológico Argentino, Junio 2014, Córdoba, T8-5.

Thiéblemont, D., Stein, G., Lescuyer, J.l., 1997. Gisements epithermaux et porphyriques: la connexion adakite: Comptes Rendus Académie Des Sciences. Sci. Terre Des Planèt. 325, 103–109.

Valencia, V.A., Ruiz, J., Barra, F., Gehrels, G., Ducea, M., Titley, S.R., Ochoa-Landín, L., 2005. U/Pb zircon and Re/Os molybdenite geochronology from La Caridad porphyry copper deposit—insights for the duration of magmatismand mineralization in the Nacozari District, Sonora, Mexico. Miner. Dep. 40, 175–191.

Willner, A.P., Gerdes, A., Massonne, H.J., 2008. History of crustal growth and recycling at the pacific convergent margin of South America at latitudes 29°–36°S revealed by a U-Pb and Lu-Hf isotope study of detrital zircon from late Paleozoic accretionary systems. Chem. Geol. 253, 114–129.

Winchester, J.A., Floyd, P.A., 1977. Geochemical discrimination of different magma series and their differentiation products using immobile elements. Chem. Geol. 20, 325–343.

Xu, J.F., Shinjo, R., Denfant, M.J., Wang, Q., Rapp, R.P., 2002. Origin of Mesozoic adakitic intrusive rocks in the Ningzhen area of east China: partial melting of delaminated lower continental crust? Geology 30, 1111–1114.

Yogodzinski, G.M., Lees, J.M., Churikova, T.G., Dorendorf, F., Wöemer, G., Volynets, O.N., 2001. Geochemical evidence for the melting of subducting oceanic lithosphere at plate edges. Nature 409, 500–504.

Zanettini, J.C., Carotti, M.A., 1993. Yacimientos metalíferos y metalogénesis. In: Ramos, V.A. (Ed.), XII Congreso Geológico Argentino y 2° Congreso de Exploración de Hidrocarburos, 4. Geología y Recursos Naturales de Mendoza Relatorio, pp. 485–504.